The Range of Spinel Compositions in Terrestrial Mafic and Ultramafic Rocks

Article *in* Journal of Petrology · December 2001

DOI: 10.1093/petrology/42.12.2279

2 authors, including:

Stephen John Barnes
The Commonwealth Scientific and Industrial Research Organisation
219 PUBLICATIONS **8,110** CITATIONS

SEE PROFILE

JOURNAL OF PETROLOGY | VOLUME 42 | NUMBER 12 | PAGES 2279–2302 | 2001

The Range of Spinel Compositions in Terrestrial Mafic and Ultramafic Rocks

STEPHEN J. BARNES[1]* AND PETER L. ROEDER[2]

[1]CSIRO—EXPLORATION AND MINING, 26 DICK PERRY AVENUE, KENSINGTON, WA 6151, AUSTRALIA

[2]DEPARTMENT OF GEOLOGICAL SCIENCES, QUEEN'S UNIVERSITY, KINGSTON, ONTARIO, CANADA K7L 3N6

RECEIVED DECEMBER 19, 2000; REVISED TYPESCRIPT ACCEPTED JUNE 13, 2001

Compositional fields for spinels from a wide variety of mafic–ultramafic igneous rock types and tectonic environments have been determined from a global database of over 26 000 analyses. These fields are defined using contoured data density plots based on the spinel prism, and plots of TiO_2 vs ferric iron, for mantle xenoliths, ophiolitic rocks, continental layered intrusions, alkalic and lamprophyric rocks, tholeiitic basalts, Alaskan ultramafic complexes and komatiites. Several trends appear regularly in the various environments: a trend of widely variable $Cr/(Cr + Al)$ at low $Fe^{2+}/(Mg + Fe^{2+})$ (the Cr–Al trend); increasing Fe^{3+}, $Fe^{2+}/(Mg + Fe^{2+})$ and TiO_2 at constant $Cr/(Cr + Al)$ (Fe–Ti trend); a trend found primarily in kimberlites, similar to Fe–Ti but at constant $Fe^{2+}/(Mg + Fe^{2+})$; and an unusual trend of increasing Al found only in layered intrusions. The Cr–Al and Fe–Ti trends are both found to varying degrees in tholeiitic basalts. The Cr–Al trend is prevalent in rocks that have equilibrated over a range of pressures, whereas the Fe–Ti trend is dominantly due to low-pressure fractionation. The most Cr-rich chromites found in nature occur in boninites, diamond-bearing kimberlites, some komatiites and ophiolitic chromitites. Exceptionally reduced chromites are found in some komatiites and in ophiolitic chromitites. Detrital chromites from the Witwatersrand conglomerates are of komatiitic provenance.

KEY WORDS: *basalt; chromite; kimberlite; ophiolite; spinel*

INTRODUCTION

Spinels have been used as 'petrogenetic indicators' since the term was first applied to them by Irvine (1965). Their usefulness stems from the fact that spinels crystallize over a wide range of conditions from mafic and ultramafic magmas and, in the case of chromites, are often among the first phases to crystallize. They also exhibit a wide range of solid solution, the thermodynamics of which has been studied extensively (O'Neill & Wall, 1987; Mattioli & Wood, 1988; Wood, 1990; Sack & Ghiorso, 1991; Poustovetov, 2000). They are relatively refractory and resistant to alteration, particularly compared with other high-temperature igneous minerals such as olivine. They occur in a high proportion of terrestrial mafic and ultramafic rocks, and a very large volume of microprobe data is available on their compositions.

Publications on spinels (particularly chromites) have routinely used compositional fields based on the spinel prism to compare populations of analyses. Some of these fields have remarkable longevity, particularly those defined for layered intrusions and Alpine peridotites by Irvine (1967, 1977). Many new data have become available in the last 20 years, however, and it has become apparent that a new compilation of data is necessary to reflect this. The prime purpose of this paper is to analyse a global database of about 26 000 spinel analyses from terrestrial igneous and metamorphosed igneous rocks, and to extract from this database the characteristic compositional fields of spinels from the wide variety of magma types and tectonic environments in which they occur. The basis for this is the spinel database described by Roeder (1994), supplemented by a body of more than 10 000 new analyses released subsequent to the Roeder (1994) compilation. The list of data sources comprises 1233 references, and it is not practical to list all of these. The complete bibliography may be downloaded from the *Journal of Petrology* Web site at http://www.petrology.oupjournals.org.

Extended dataset can be found at
http://www.petrology.oupjournals.org

*Corresponding author. E-mail: Steve.Barnes@csiro.au

The major focus of the paper is on spinels in igneous rocks. However, a large proportion of these rocks have been metamorphosed, and igneous spinel compositions have been obscured by a veil of metamorphic effects. We have therefore included a compilation of demonstrably metamorphic spinel compositions, to illustrate the clear contrast and emphasize the need to take metamorphic effects into account.

Full discussion of the implications of the data is beyond the scope of this paper, and would duplicate extensive discussions elsewhere [see review by Roeder (1994) and references therein]. Brief summaries only are given of the nature and possible interpretations of the major trends, and some illustrative examples of applications are given at the end of the paper.

Data density plots

Publications on spinels have routinely used compositional 'fields' based on the spinel prism (Stevens, 1944) to compare populations of spinel analyses. The approach used in this paper is that of 'data density contour plots' (DDCPs), or 'fried egg diagrams' as they have been called, based on two common projections of the spinel prism: the Cr–Al–Fe^{3+} triangular plot, representing projection onto the end face of the prism, and the plots of $Cr/(Cr + Al)$ and $Fe^{3+}/(Cr + Al + Fe^{3+})$ vs $Fe^{2+}/(Mg + Fe^{2+})$. In addition, plots of TiO_2 content against $Fe^{3+}/(Cr + Al + Fe^{3+})$ are used, Ti being the one minor spinel constituent for which a large volume of reasonably reliable data exists. Other elements, such as Zn, Mn, V and Ni, may also contain important information, but many of the published data on minor elements are of indeterminate quality. These elements were therefore not considered.

The data density approach involves contouring these various plots for concentration of data, such that the nth percentile contour encloses the most densely packed n% of the data. This approach is useful in analysing very large data populations as presented here, where there are heavy concentrations of clustered data points surrounded by abundant outliers. Simple x–y plots tend to focus attention on outlying data points rather than giving a clear impression of where the bulk of the data points lie. The data density approach is the best way to derive a meaningful compositional field from a population.

Data density plots are calculated as follows. For each point on a particular x–y plot, a box is centred on that point having a width of 0·1 ratio units of $Cr/(Cr + Al)$, $Fe^{2+}/(Mg + Fe^{2+})$, etc. (or ~10% of the observed range in TiO_2 on the Ti–Fe^{3+} plots). On the triangular plots, the box is replaced by a triangle 0·1 ratio units on the side (i.e. 10% of the size of the whole triangle). The total number of points within the dataset that fall within that box is counted. This procedure is applied to every datum in the set, and the data are then ordered according to the 'number in box' score. These are then assigned a percentile value and contoured by hand. The calculation was carried out using Visual Basic macros in Microsoft Excel.

The DDCP approach requires large data populations to make it meaningful. The minimum data subset for which density contours are shown is 148 analyses, the median number is 528 and the maximum 2781 (Table 1). Furthermore, the dataset should not be dominated by a single locality, particularly if this locality is not entirely representative of the category. To this end, if any individual data source (defined in terms of a source publication) contained >10% of the total population in the category or subcategory in question, data points were randomly selected from this source to reduce the sample size to 10% of the total and reduce bias. This ensures that a wide range of localities was included in the sample. (In one case, that of Hawaiian lava lakes, a large enough dataset was available from one distinctive locality to justify breaking this out as a subcategory on its own).

Even with these criteria satisfied, there is still the limitation that the only samples represented are those that somebody has seen fit to analyse. Given that researchers tend to be drawn to the unusual rather than the mundane, this introduces a bias towards greater variability and diversity. There is probably a bias in the dataset towards chromites and away from magnetites, exacerbated by the fact that Ti-bearing magnetites in mafic plutonic rocks are commonly exsolved and therefore difficult to analyse. Nothing can be done about this, and it should be kept in mind.

This paper presents a large number of data density plots, and defines 50th and 90th percentile contours for data from a wide range of environments. These contours can be used as a quantitative basis of comparison of one environment with another, or for such applications as identifying the affinities of lavas or intrusions in poorly characterized terrains, or identifying the provenance of detrital assemblages. Some examples are given in the concluding section.

Database

The approach used was to classify all data points into a two-level hierarchical grouping, as specified in Table 1. The major categories are mantle nodules or xenoliths; 'oceanic' plutonic rocks (incorporating ophiolites, Alpine ultramafic complexes and ocean-floor ultramafic rocks); continental mafic intrusions; Alaskan zoned ultramafic complexes; tholeiitic basalts; alkalic and lamprophyric rocks (including kimberlites); komatiites; and metamorphic spinels. A minor category of detrital spinels is also

Table 1: Listing of data categories and subcategories, with number of analyses represented

Category and subcategory	No. of references	Analyses
Alaskan ultramafic complexes	7	386
*Alkaline rocks, alkali basalts and lamprophyres (*sensu lato*)*		
Alkali basalts, including basanites and phonolites	44	597
Kimberlites (excluding xenoliths or nodules)	43	1693
Lamproites	16	148
Lamprophyres (excluding kimberlites and lamproites)	10	67
Ultrapotassic lavas including shoshonites	13	123
Tholeiitic basalts and boninites		
Boninites	27	528
Continental flood basalts	30	582
Hawaii lava lake samples	3	445
Island arc	39	1154
Ocean floor	83	1855
Ocean island	33	451
Ophiolites (ophiolitic basalts, probably including some boninites)	7	52
Undefined	44	752
Detrital		
Witwatersrand detrital spinels	1	101
Komatiites (magnetite rims excluded)		
Amphibolite facies terrains, Al-undepleted komatiites	7	1082
Amphibolite facies terrains, Al-depleted komatiites	2	358
Greenschist terrains, Al-undepleted komatiites	8	1134
Sulphide (margins of massive Fe–Ni sulphide orebodies)	3	707
Continental mafic–ultramafic intrusions		
Chromitites (stratiform, in layered intrusions)	27	681
Layered intrusions, excluding chromitites	79	2594
Subvolcanic sills and dykes (flood basalt provinces, including Pechenga)	16	813
Metamorphic spinels		
In high-grade metasediments	50	341
Magnetite rims on chromites in komatiites (greenschist facies)	2	180
Magnetite rims on chromites in komatiites (amphibolite facies)	2	1607
Ophiolites, Alpine peridotites and oceanic peridotites		
Chromitites	90	1859
High-*P* Alpine	16	373
Ocean-floor peridotites	29	440
Ophiolitic ultramafic rocks excluding chromitites	121	2781
Mantle and lower-crustal xenoliths		
In basalts	77	932
In island-arc volcanic rocks	13	160
In kimberlites	39	409
Unspecified	83	912
Total	981	26 297

included. These are further subdivided into subcategories. DDCPs are presented for each category and for each subcategory for each of the four spinel compositional plots. Coordinates for the data density contours on each plot may be downloaded from the *Journal of Petrology* Web site at http://www.petrology.oupjournals.org.

Database manipulation was carried out using a Microsoft Access relational database. Each analysis was assigned to a three-level classification, based on the title and keywords of the source publication, and the host rock type where known. The category breakdown (first and second levels) is defined in Table 1. Overlapping categories are not permitted; for example, alkali basalts from ocean islands are included only in the alkali basalt subcategory of the 'alkali basalts and lamprophyres' category, and not in the 'ocean islands' category of 'basalts'. However, the database is flexible enough to allow different combinations, such that (to extend the example) alkali basalts can be compared globally with tholeiitic basalts regardless of environment.

An important uncertainty that must be mentioned at the outset is the uncertainty in the ferric iron content of spinel. In all cases, we have taken the approach of calculating ferric iron based on the assumption of stoichiometry. The ferric iron content of each analysis was determined by assuming stoichiometry, and an ideal XY_2O_4 formula where X = (Fe^{2+},Ni,Mn,Co,Zn) and Y = (Cr^{3+},Fe^{3+},Al). Ti is assumed to be present as an ulvöspinel component, and V is assigned to a fictive $Fe_7V_2O_{12}$ component. Iron is subdivided into ferrous and ferric to satisfy the condition $n_Y = 2n_X$ where n_Y is total atoms of trivalent cations, and n_X is total divalent cations per unit cell. The drawback of stoichiometry-based calculation methods is that errors in all the major elements propagate into significantly larger errors in the estimated Fe^{3+} (Wood & Virgo, 1989), and this error may be a significant component of the observed variance in trivalent ions. There is nothing that can be done about this, other than to recognize it as a limitation in interpreting relatively small variations in ferric iron content.

One of the major difficulties with the classification scheme is in separating igneous spinels from metamorphosed or metamorphogenic spinels. Most of the latter fall into the compositional field of magnetite, separated from Cr-rich spinels by a compositional minimum as discussed below, and one possible solution to the problem was to exclude all magnetites from consideration and restrict the analysis to Cr-rich spinels alone. This proved impractical, as in many environments there is a complete compositional spectrum from chromite to magnetite, and excluding magnetite would have involved making an entirely arbitrary distinction with a profound impact on the resulting data density fields. We have therefore taken the approach of including all spinels, but breaking out demonstrably metamorphic compositions into a separate category under the heading of 'metamorphic spinels'.

The complete database, including all references to data sources, exists in Microsoft Access format, and a copy can be obtained from S.J.B. by sending a self-addressed envelope and a blank CD-ROM.

TRENDS IN SPINEL COMPOSITIONAL SPACE

A number of distinctive features reappear regularly in the various datasets, and it is useful to summarize them at the outset and to establish some shorthand terminology. More detailed discussion of the nature and causes of these features has been given by Roeder (1994), and below in the descriptions of the various categories. These features are illustrated in Fig. 1, superimposed on data density contours for the entire database covered by this paper, reduced to 21 644 samples after filtering for overrepresented localities.

The spinel gap

A data density minimum is evident in almost every data grouping between chrome-rich spinels (usually chromites) and Fe^{3+}-rich spinels approaching magnetite compositions. This has two separate causes: the extensive solvus in the spinel solid solution (Mattioli & Wood, 1988; Nell & Wood, 1989; Sack & Ghiorso, 1991) and the well-known reaction relationship in igneous rocks between chromite and Cr-bearing pyroxenes, particularly clinopyroxenes. This reaction relationship causes the cessation of crystallization of chromite, and a subsequent gap before the onset of crystallization of magnetite, in typical basaltic suites and layered mafic–ultramafic intrusions such as the Bushveld Complex (Roeder, 1994). This crystallization gap is not universally present, however, as discussed below.

The Cr–Al trend

The global dataset shows a trend of widely variable Cr/(Cr + Al) at generally low Fe^{2+}/(Mg + Fe^{2+}) (Fig. 1b), and at low concentrations of Fe^{3+} and TiO_2, with an overall tendency toward increasing Cr/(Cr + Al) with increasing Fe^{2+}/(Mg + Fe^{2+}). This sloping trend was first described by Irvine (1967), who explained that lines parallel to this trend correspond to spinels equilibrating with olivine of constant composition at constant temperature. The slope of the trend is a consequence of non-ideality within the spinel solid solution, and the temperature dependence of this line is the basis of the

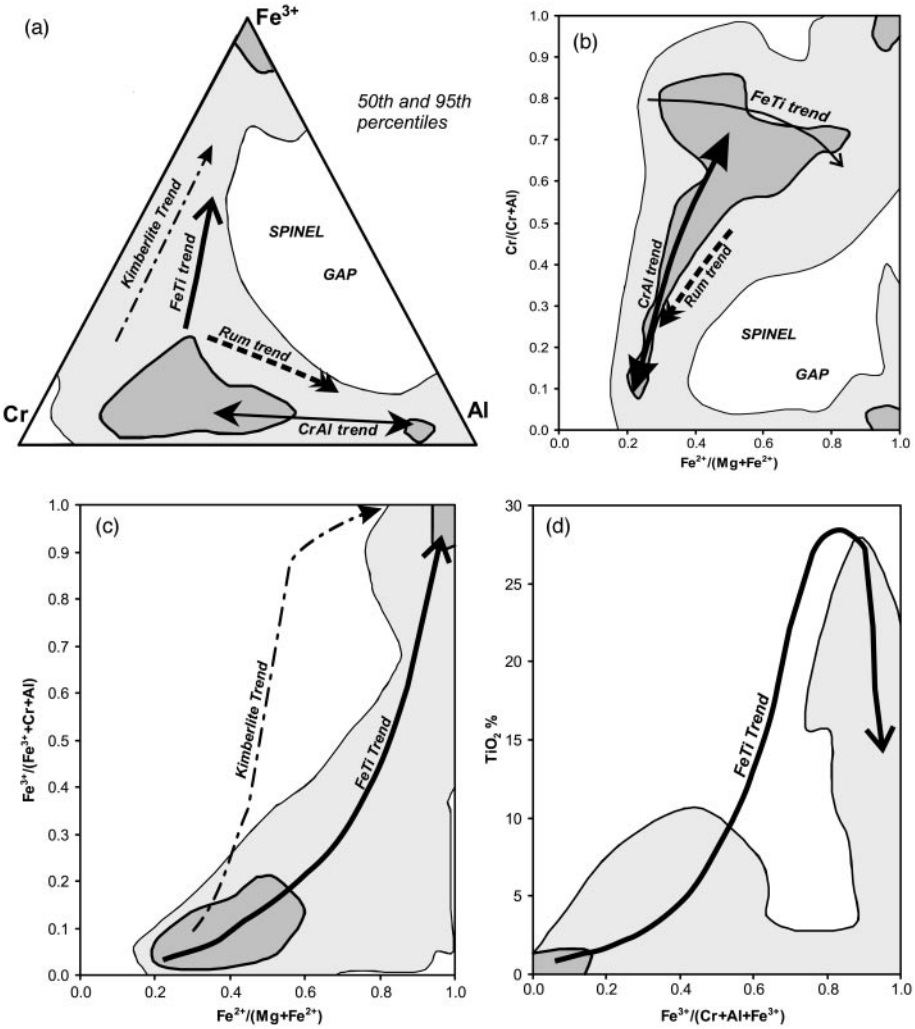

Fig. 1. The entire terrestrial spinel dataset (corrected for over-represented localities) of 21 644 analyses covered by this study, contoured on the plots used throughout this paper. The spinel gap and generalized trends discussed in the text are labelled. Contours in these and subsequent plots enclose the most densely packed 50% (heavy line, dark shading) and 90% (light line and shading) of the data points.

olivine geothermometer (Sack & Ghiorso, 1991; Poustovetov, 2000). The lower limit of $Fe^{2+}/(Mg + Fe^{2+})$ for a given $Cr/(Cr + Al)$ is determined by the upper limit of the Mg/Fe ratio of mantle olivines.

The sloping $Cr/(Cr + Al)$ vs $Fe^{2+}/(Mg + Fe^{2+})$ relationship is referred to here as the Cr–Al trend. It is particularly evident in the various mantle and lower-crustal samples (xenoliths, ophiolites and ocean-floor peridotites), and in some types of basalt. In the case of high-pressure plutonic samples it is probably the result of equilibria between Al-bearing pyroxenes and Mg–Al-rich spinels. In lavas the interpretation is more complex, and relates to the Al and Cr contents of the melt (Roeder & Reynolds, 1991), as discussed further below in the context of basalts.

The Fe–Ti trend

Data on Cr-rich spinels from some groups of basalts and from most differentiated mafic–ultramafic igneous bodies show a trend of increasing Fe^{3+} and $Fe^{2+}/(Mg + Fe^{2+})$ that curves up towards magnetite (Fig. 1a–c), and that is typically accompanied (at least up as far as moderately magnetite-rich spinels) by increasing TiO_2 (Fig. 1d). This trend can be attributed to evolution of spinel compositions during fractional crystallization of olivine or pyroxene (with or without plagioclase) from the host magma, which increases the Fe/Mg ratio and the Ti content of the melt. In many cases this is accentuated by reaction of spinels in orthocumulate rocks with evolving trapped intercumulus magma (Henderson, 1975; Henderson & Wood, 1981; Roeder & Campbell, 1985; Scowen *et al.*,

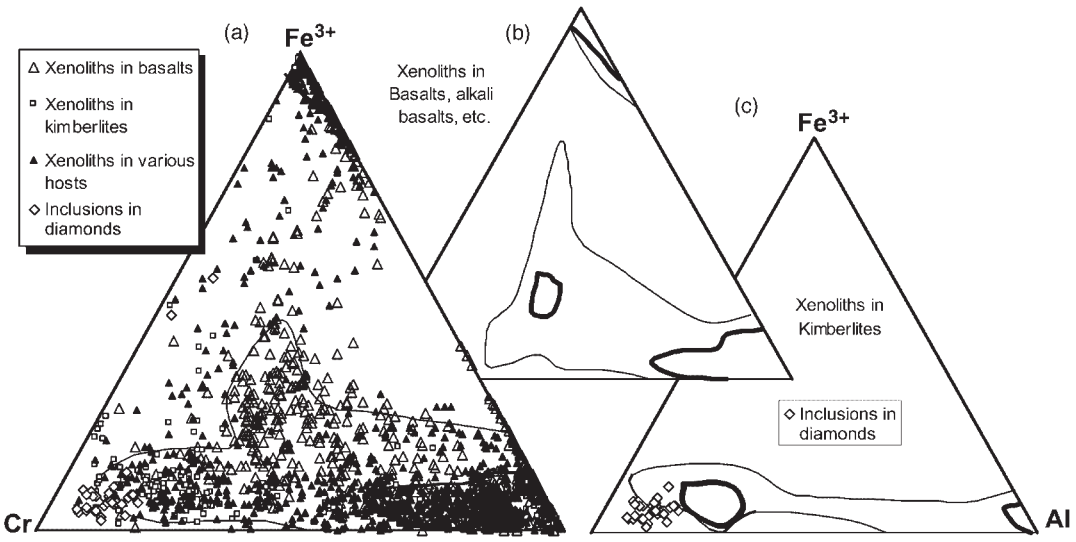

Fig. 2. Trivalent ion plots for ultramafic nodules and high-*P* xenoliths. (a) All data points, data density contours on complete dataset. (b) Xenoliths in all lithologies (primarily alkali basalts) except kimberlites. (c) Contours on data from xenoliths in kimberlites, excluding spinel inclusions in diamonds shown as individual data points.

1991). The variation in $Fe^{2+}/(Mg + Fe^{2+})$ has two sources: evolving melt compositions during crystallization, and the exchange of Fe^{2+} and Mg between spinel and coexisting silicates (usually olivine), which favours increasing $Fe^{2+}/(Mg + Fe^{2+})$ in spinel with falling temperature (Irvine, 1965). This effect is most pronounced in slowly cooled rocks.

The kimberlite trend

This is similar to the Fe–Ti trend, in being a trend of increasing Fe^{3+} and TiO_2 at nearly constant $Cr/(Cr + Al)$, but differs in maintaining nearly constant $Fe^{2+}/(Mg + Fe^{2+})$ over a wide range in Fe^{3+} (Fig. 1a and c). It is most evident in kimberlites and to a lesser extent in alkali basalts, and reflects the generally high ratio of Fe^{3+} to Fe^{2+} in these rocks, as discussed further below. The increase in Ti is a secondary consequence of the increased tendency of Ti to partition into spinels with higher magnetite contents.

The Rum trend

This unusual trend, initially observed by Henderson (1975) and Henderson & Wood (1981) in the Rum layered intrusion, is restricted to mafic layered intrusions, where Cr-spinels occur within gabbroic orthocumulate rocks. It involves an increase in Al mainly at the expense of Cr with some decrease in Fe^{3+} (i.e. a trend roughly towards the Al apex on the triangular cation plot), accompanied by decreasing $Fe/(Mg + Fe^{2+})$ (Fig. 1a and b), and has been attributed to reaction between cumulus chromite, trapped intercumulus liquid, plagioclase and olivine. The decrease in Fe with falling temperature is the opposite trend from normal. It arises from the compositional effect of the changing Cr/Al ratio in the spinel on the activity coefficients of Fe^{2+} and Mg, and the resulting change in Fe/Mg exchange coefficient (K_d) with silicates. Accessory chromites in cumulates are buffered by the compositions of the cumulus silicate phases; as K_d values change with falling temperature and silicate Fe/Mg ratios remain relatively constant, the Fe/Mg of the spinel is constrained to decrease as its Cr/Al ratio falls. Both the Rum trend and the Fe–Ti trend may be seen in the same samples depending on the micro-environment of the chromite grains.

DATA PRESENTATION

A consistent scheme is used throughout the paper. Four plotting schemes are used for each dataset: the $Cr–Al–Fe^{3+}$ triangular plot, representing projection onto the end face of the spinel prism; the longitudinal spinel prism projections of $Cr/(Cr + Al)$ and $Fe^{3+}/(Cr + Al + Fe^{3+})$ vs $Fe^{2+}/(Mg + Fe^{2+})$; and TiO_2 vs $Fe^{3+}/(Cr + Al + Fe^{3+})$. For each major category we show a single plot with all individual data points and contours over the whole dataset, and DDCPs only (with data points as well in cases where we have a small group of analyses) for each of the subcategories. In most cases the major category plots include a number of data points that are undefined or belong to small subcategories not represented by plots. The categories are discussed broadly in order of decreasing pressure: probable mantle (or deep

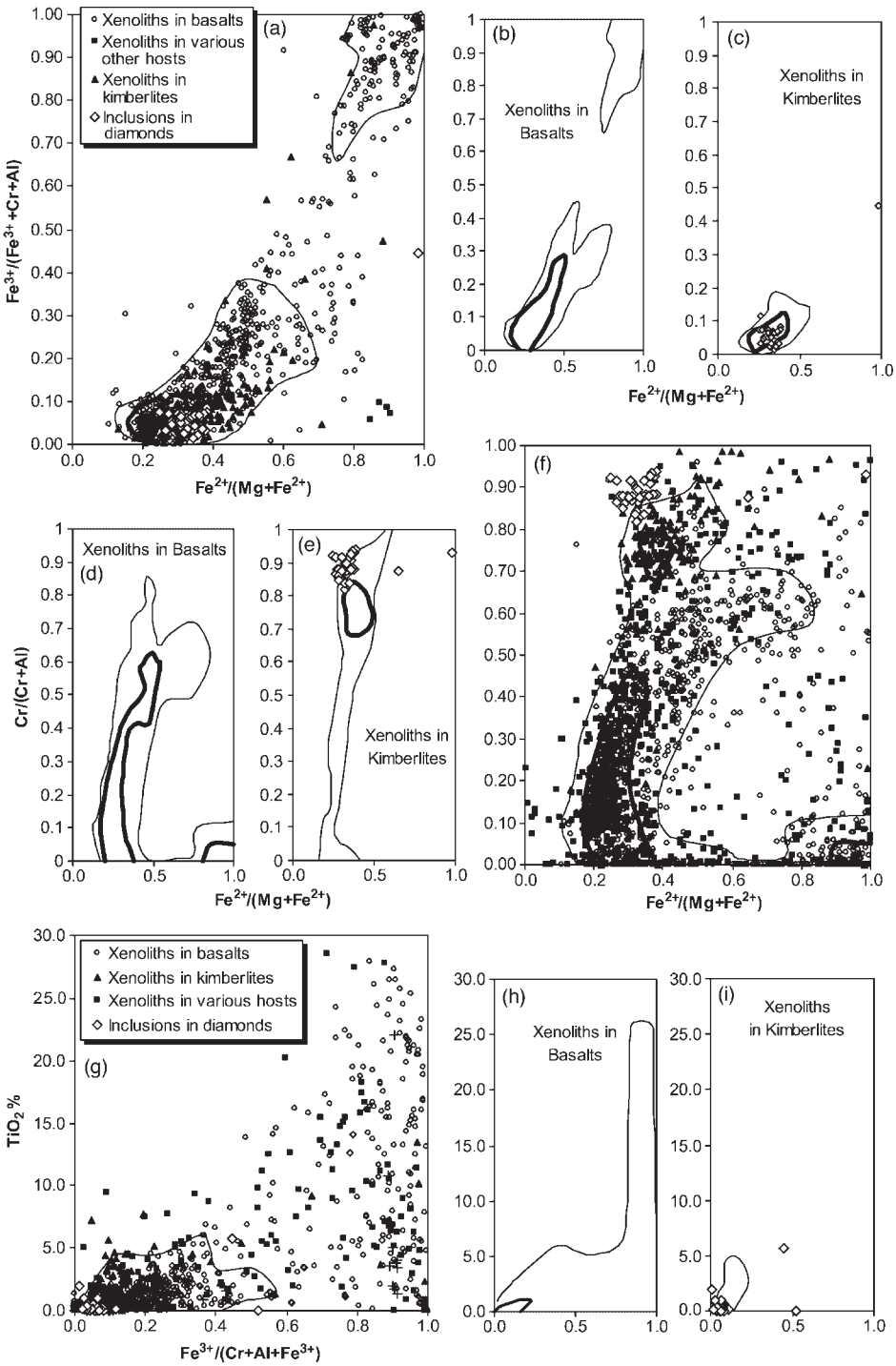

Fig. 3. $Fe^{3+}/(Cr + Al + Fe^{3+})$ vs $Fe^{2+}/(Mg + Fe^{2+})$, $Cr/(Cr + Al)$ vs $Fe^{2+}/(Mg + Fe^{2+})$ and TiO_2 vs $Fe^{3+}/(Cr + Al + Fe^{3+})$ plots for ultramafic nodules and high-*P* xenoliths; groupings as in Fig. 2. Chromite inclusions in diamonds shown as individual data points in sub-plots (c), (e) and (i).

crustal) samples, oceanic and continental plutonic rocks, and various categories of mafic and ultramafic lavas. Metamorphic spinels (including magnetite rims) are treated as a separate category.

Mantle nodules and high-*P* xenoliths

This category includes samples of mantle or lower-crustal material carried to the surface as xenoliths (commonly referred to as 'nodules') in deep-seated mafic and

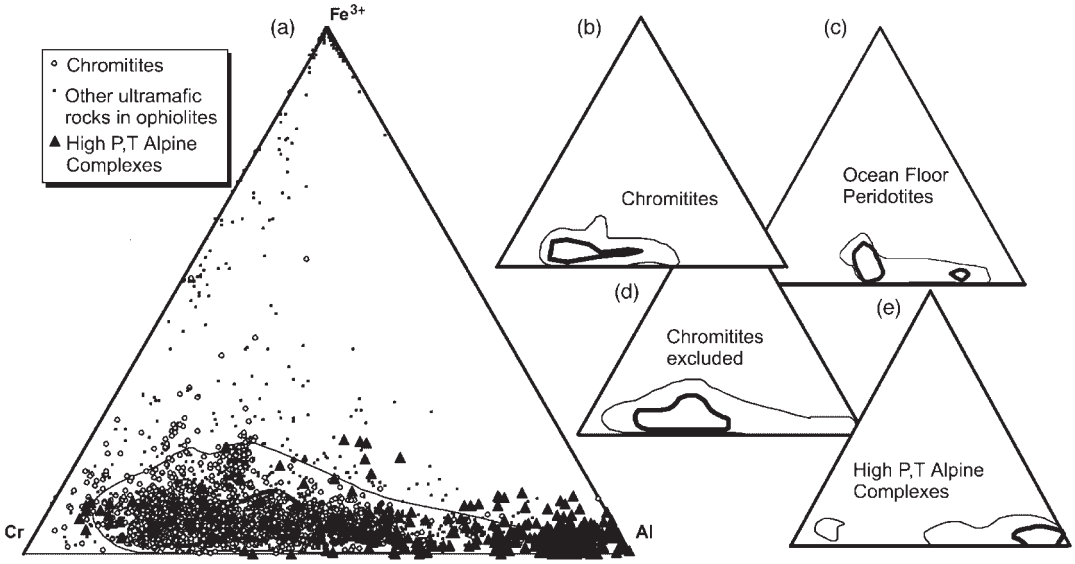

Fig. 4. Trivalent ion plots for ophiolites, 'Alpine ultramafics' and abyssal (ocean-floor) peridotites. (a) All data points, and contours on complete dataset; (b) data from chromitite seams only; (c) ocean-floor peridotites; (d) data from ophiolites excluding chromite seams; (e) high-pressure metamorphosed and tectonized 'Alpine ultramafic' complexes.

ultramafic magmas, namely alkali basalts and their kin, and kimberlites.

The dataset as a whole shows a strong Cr–Al trend and a small spinel gap (Figs 2 and 3). The Cr–Al trend is strongly developed both in xenoliths from kimberlites (Fig. 3c) and those from mafic lavas (Fig. 3b), from high-*P*, Mg–Al spinel *sensu strictu* compositions at one end to typical Fe^{3+}-poor chromites at the other. This can be interpreted as a high- to low-pressure trend, spinel compositions being controlled by Al exchange with coexisting pyroxenes. The low Cr/(Cr + Al) in some mantle nodules may be the result of clinopyroxene–spinel subsolidus equilibration where a significant amount of Al is exsolved from clinopyroxene to form aluminous spinel. Textural evidence for this was noted by Sinton (1977) in peridotite from Red Mountain, New Zealand.

Xenoliths in kimberlites contain some very Cr-rich chromites, and some of the most Cr-rich chromites found in nature are found as inclusions in diamonds. These chromites have very high Cr/(Cr + Al) and low ferric iron and TiO_2 (Fig. 3c). A likely explanation for this is equilibration with Cr-bearing garnets at very high pressure. There is some degree of overlap between diamond inclusions and chromites from boninites and Al-depleted komatiites, discussed below.

Xenoliths in alkali basalts show a much less developed trend, which may be the result of superimposition of an Fe–Ti or kimberlite trend on the Cr-rich end of the Cr–Al trend. Alkali basalt xenoliths also contain a substantial proportion of Ti-rich magnetite (Fig. 3g and h), possibly reflecting a component of cognate xenoliths developed during fractionation or contamination by host lava.

Ophiolites, Alpine peridotites and oceanic peridotites

This category is representative of plutonic ultramafic (and some mafic) cumulate rocks of broadly oceanic affinity, and includes tectonically emplaced high-pressure, high-temperature 'Alpine' ultramafic bodies of probable ophiolitic affinities in orogenic belts. The ophiolite subcategory includes both the mantle and lower-crustal component of ophiolites, and both magma chamber cumulates and tectonized mantle restites. Ultramafic rocks dredged or cored from the ocean floor are also included within this category.

The dataset is dominated by a strong Cr–Al trend, from Al-rich spinel (*sensu stricto*) in high-pressure spinel lherzolite bodies to Fe^{3+}-poor chromitites in refractory podiform and stratiform bodies (Figs 4 and 5). Chromitites have a lower and more restricted range of $Fe^{2+}/(Mg + Fe^{2+})$ compared with rocks containing lower proportions of chromite, owing to the less pervasive effect of re-equilibration with olivine. A similar trend, but not extending as far towards Cr-rich chromites, is seen in dredged or drilled ocean-floor peridotite samples (Figs 4c and 5e and i). This group extends to even lower values of $Fe^{2+}/(Mg + Fe^{2+})$ than the chromitites, reflecting the high temperature of equilibration with olivine. Ti contents are consistently

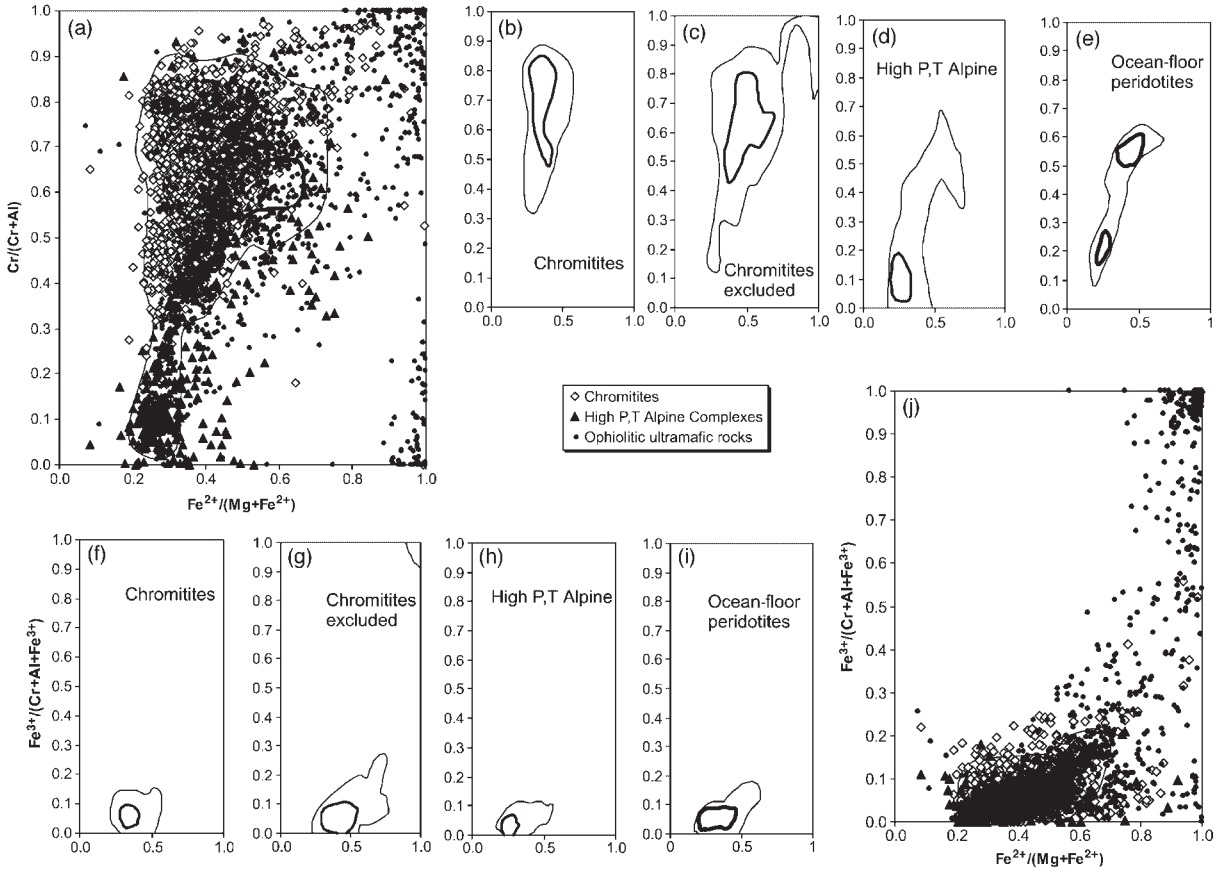

Fig. 5. $Fe^{3+}/(Cr + Al + Fe^{3+})$ vs $Fe^{2+}/(Mg + Fe^{2+})$ and $Cr/(Cr + Al)$ vs $Fe^{2+}/(Mg + Fe^{2+})$ for ophiolites, 'Alpine ultramafics' and abyssal (ocean-floor) peridotites; categories as in Fig. 4.

low (Fig. 6), with the highest values in ophiolitic magma chamber rocks (Fig. 6c). A number of factors are likely to be at play in producing these trends, including the effect of pressure on Cr partitioning between spinel and silicate phases (pyroxene and garnet), and the variation in bulk-rock composition from relatively Al-rich 'fertile' lherzolite to Al-poor refractory harzburgites (Bonatti & Michael, 1989).

Continental mafic intrusions

The DDCPs for layered mafic–ultramafic intrusions are substantially different depending on whether chromitites are included in the dataset. The category as a whole shows a very clearly defined spinel gap, and a combination of a strong Fe–Ti trend and a less prominent Rum trend (Figs 7 and 8). These features are due to changing magma chemistry as a result of fractionation within the crust, combined with a strong overprint owing to reaction between accessory cumulus spinel grains and evolving trapped intercumulus liquid (Henderson, 1975; Henderson & Wood, 1981; Roeder & Campbell, 1985; Scowen *et al.*, 1991). Chromitites are strongly clustered at relatively low Fe^{3+} contents, with less extensive development of an Fe–Ti trend (Figs 7d and 8c, f and l). The contrast is due to a buffering effect: chromite is less susceptible to trapped liquid reaction effects when the proportion of chromite to liquid in the rock is very high. The compositional field of chromitites therefore closely matches compositions of primary liquidus chromites. The 90th percentile field for the non-chromitite dataset (Figs 7c and 8b, e and k) extends to the Cr–Fe join, and includes some metamorphic ferritchromit compositions (see below).

Included in this category are subvolcanic mafic intrusions from continental flood basalt terrains, mainly from the Siberian and Karoo flood basalt provinces, and including the Noril'sk and Talnakh intrusions in Siberia and the Insizwa (Mt. Ayliff intrusion) in the Karoo (Eales, 1979; Cawthorn *et al.*, 1991; Barnes & Kunilov, 2000) (Figs 7d and 8d, g and m). They show a very strongly developed Fe–Ti trend, and

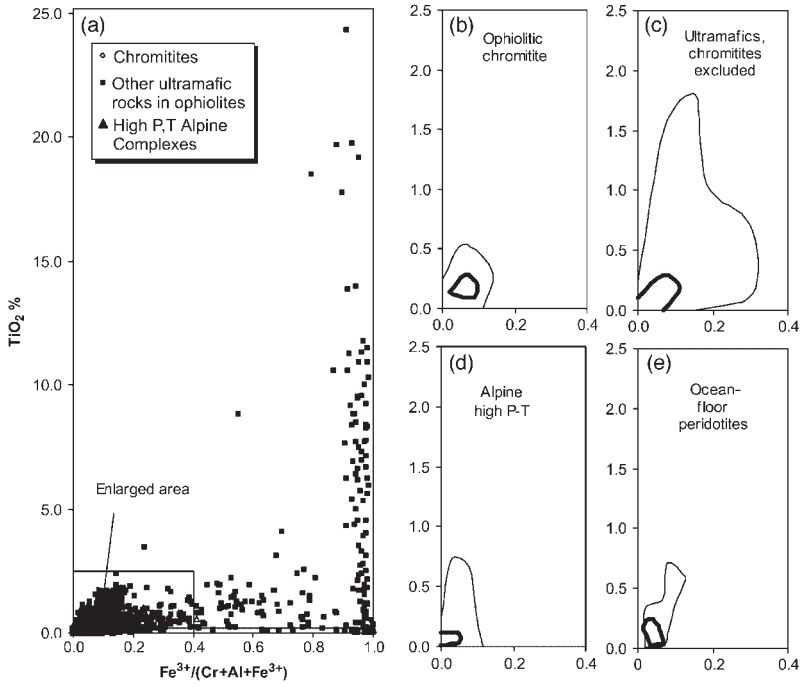

Fig. 6. TiO_2 vs $Fe^{3+}/(Cr + Al + Fe^{3+})$ plot for ophiolites, 'Alpine ultramafics' and abyssal (ocean-floor) peridotites; categories as in Fig. 4. [Note the scale change in (b)–(e).].

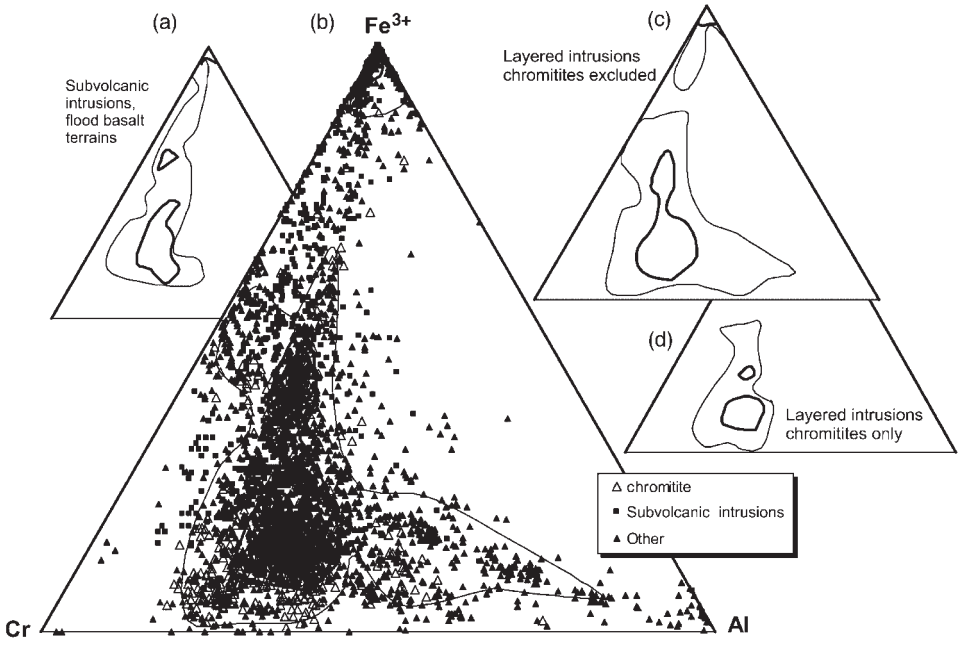

Fig. 7. Trivalent ion plots for continental mafic intrusions. (a) Subvolcanic intrusions from flood basalt terrains; (b) all data points and contours on complete dataset; (c) layered intrusions excluding subvolcanic intrusions in (a), and excluding chromitite samples; (d) chromitite seams only.

characteristically Ti-enriched chromites and magnetites, attributable to a combination of extensive trapped liquid reaction and variable degrees of low-pressure fractionation. An interesting feature of this subcategory is the similarity with spinels from flood basalts themselves, as discussed below.

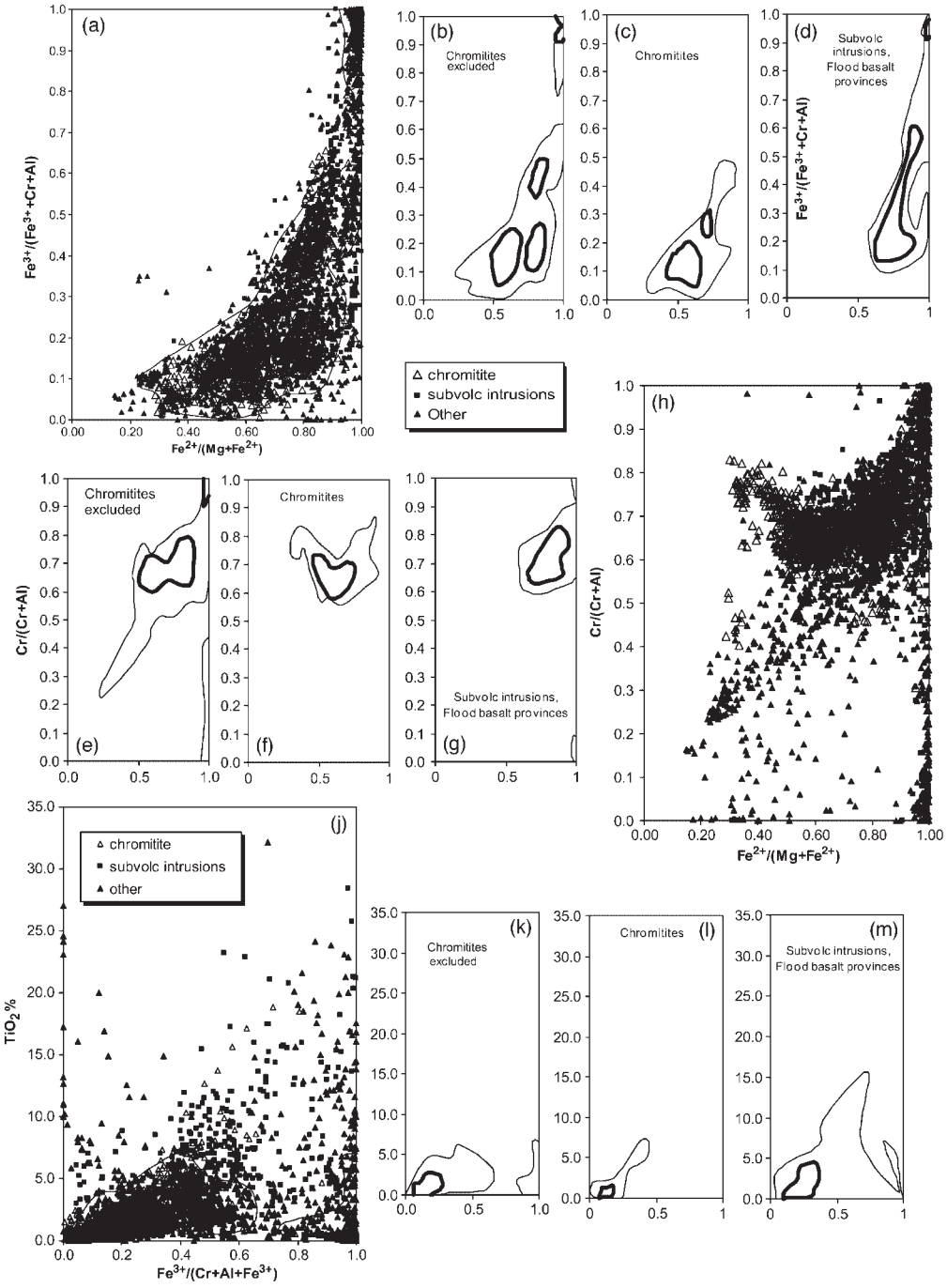

Fig. 8. $Fe^{3+}/(Cr + Al + Fe^{3+})$ vs $Fe^{2+}/(Mg + Fe^{2+})$, $Cr/(Cr + Al)$ vs $Fe^{2+}/(Mg + Fe^{2+})$and TiO_2 vs $Fe^{3+}/(Cr + Al + Fe^{3+})$ for continental mafic intrusions, subdivided as in Fig. 7.

A recent paper on detrital spinels from Rum (Power *et al.*, 2000) points out that some existing discriminant fields represent biased datasets, and emphasizes the importance of considering disseminated chromite compositions in sedimentary provenance studies. The compositional fields in Figs 7 and 8 bear this out. Chromites derived from layered intrusions should be distinguishable from ophiolitic, komatiitic and other provenances provided that it is recognized that chromitites contribute only a small proportion of the

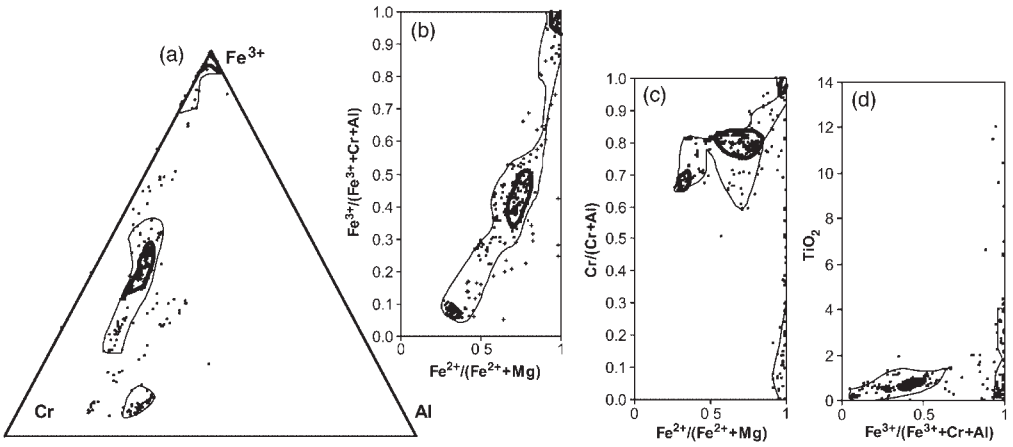

Fig. 9. Spinel prism projections and TiO_2 vs $Fe^{3+}/(Cr + Al + Fe^{3+})$ plots for Alaskan zoned ultramafic complexes.

chromite present within layered intrusions. The 'chromitites excluded' fields in Figs 7 and 8 are more appropriate to provenance studies, and the same applies to the ophiolite data in Figs 4 and 5.

Alaskan zoned ultramafic complexes

This dataset is limited to a relatively small number of analyses, but a clear Fe enrichment trend is evident (Fig. 9). This differs from the typical Fe–Ti trend in that Ti is not strongly enriched except in a small proportion of magnetite grains (Fig. 9d). Ti enrichment may be limited by competition for Ti with other phases such as amphibole, which are more common in this environment than in other continental layered mafic intrusions. There is a continuity in compositions from Cr-rich chromites right across to magnetites, a feature that reflects a combination of trapped liquid reaction and oxidation.

Tholeiitic basalts and boninites

Spinels in tholeiites (Figs 10–13) have a strongly bimodal distribution between chromites and magnetites, although spinel compositions extend across the complete spectrum. Chromites span a wide range in $Cr/(Cr + Al)$ and Fe^{3+}, combining elements of both the Cr–Al and Fe–Ti trends. The Cr–Al trends are most evident in the mid-ocean ridge basalts (MORBs) and island-arc tholeiites (Figs 10b and g, and 12b and g). Roeder & Reynolds (1991) demonstrated that $Cr/(Cr + Al)$ in basaltic spinels is dominantly controlled by liquid composition, which in turn is controlled by degrees of partial melting, degree of depletion of the mantle source, and fractional crystallization of chromite, olivine, plagioclase and pyroxene. It is likely that the Cr–Al trend is at least in part inherited from mantle equilibria (Dick & Bullen, 1984), but there is a substantial overprint as a result of low-pressure plagioclase fractionation and also rapid growth of chromian spinel in some lavas (Roeder *et al.*, 2000). The Fe–Ti trend (Fig. 13) is purely a low-pressure fractionation effect.

The Fe–Ti trend dominates in continental flood basalts (Figs 10d, 11d, 12d and 13d), to the point where spinels with roughly equal proportions of Cr, Al and Fe^{3+} fall within the 50th percentile, and Mg contents are substantially lower than in all other basalt groups. Spinels of this composition are rare in virtually all other terrestrial environments, with one notable exception: subvolcanic intrusions in flood basalt provinces (Figs 7a, and 8d, g and m). The strongly evolved, oxidized nature of these spinels is presumably a consequence of parent magma chemistry. The probable explanation is that these magmas have interacted to varying degrees with continental crust through contamination and assimilation. 'Primitive' high-Cr, high-Mg spinels are rare in this group, although they are found as chromite inclusions in phenocryst olivines in picritic flood basalts; for example, the Gudchichinsky suite of the Siberian Traps (Barnes & Kunilov, 2000).

Ocean-island tholeiites (Figs 10f, 11e, 12e and 13e) also show a strong Fe–Ti trend, but are more weighted towards typical chromites.

Boninites define a field of exceptionally high $Cr/(Cr + Al)$, low Fe^{3+} and exceptionally low Ti, distinct from most of the basalts and similar only to the most Cr-rich end of the ranges in island-arc tholeiites and komatiites. The boninite plots also show individual data points for 'ophiolitic basalts', these being otherwise unclassified basalts from ophiolite complexes. There is a strong overlap with the boninite field, and many of these samples are probably boninites. The origin of the distinctive

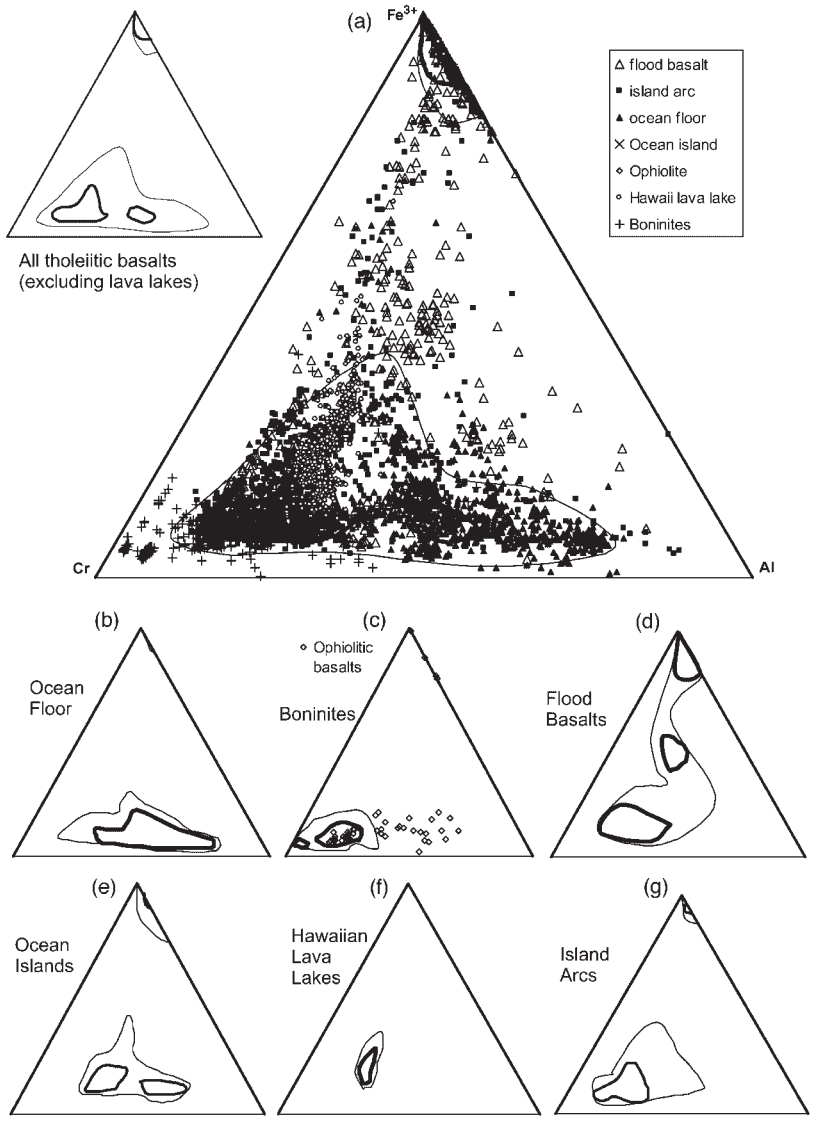

Fig. 10. Trivalent ion plots for tholeiitic basalts and boninites. Contours in (a) refer to complete dataset; (b) MORB and back-arc ocean-floor basalts; (c) boninites, with unclassified ophiolite-related basalts as individual data points (contour refers to definite boninites only); (d) continental flood tholeiites; (e) ocean-island tholeiites, excluding lava lake samples; (f) Hawaiian lava lake samples (mainly Kilauea Iki); (g) island-arc tholeiites.

population of spinels in boninites is discussed further below.

The Hawaiian lava lake group (Figs 10e, 11f, 12f and 13f) is dominated by the study of Scowen *et al.* (1991), which demonstrated a well-developed Fe–Ti trend as a result of trapped liquid reaction in the lava lake. This is particularly evident in those chromites that were not enclosed in olivine grains.

Magnetites in the tholeiitic basalts are generally Ti rich, in some cases extremely so. The strongest tendency to Ti-rich magnetites is in flood basalts (Fig. 13d), and to a lesser extent in island-arc tholeiites (Fig. 13g). The wide range in Ti contents in both is attributable to variation in the point at which ilmenite becomes a liquidus phase, competing with magnetite for Ti.

Alkali basalts and lamprophyres

This grouping incorporates all alkalic, peralkalic, potassic and ultrapotassic lavas, including all lamprophyres, following the lead of Rock (1986) in taking this term to include lamproites and kimberlites. Plutonic alkaline rocks are not included.

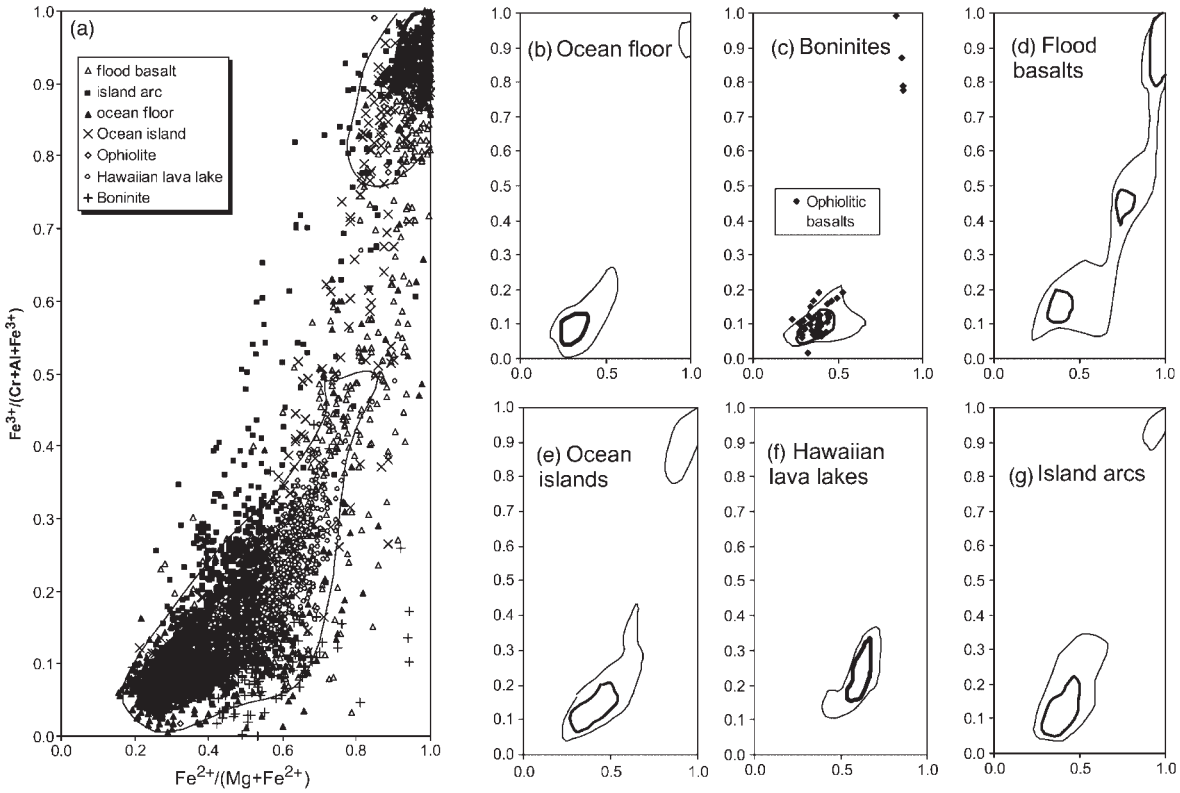

Fig. 11. $Fe^{3+}/(Cr + Al + Fe^{3+})$ vs $Fe^{2+}/(Mg + Fe^{2+})$ plots for tholeiitic basalts and boninites; subcategories as in Fig. 10.

The alkali basalt group is the most scattered of any of the datasets studied, having compositions all over the spinel prism (Figs 14 and 15) and with a very wide range of Ti contents (Fig. 15i–l). The data are strongly bimodal, with 50th percentile groupings in the Al-bearing magnetite and Al-poor chromite areas. The kimberlite dataset shows a similar range of compositions, but a much better defined characteristic 'kimberlite trend' of widely variable $Fe^{3+}/(Cr + Al + Fe^{3+})$ for a limited range of $Fe^{2+}/(Mg + Fe^{2+})$ (Fig. 15c), extending up to unusually Mg-rich magnetites and magnesioferrites, which are unique to kimberlites. Kimberlites are distinctive in having a complete range from Mg-rich aluminous titanian magnetite to Mg-rich chromite falling within the 90th percentile (Fig. 15c and f). The Mg- and Cr-rich end of the trend consists of chromites associated with diamondiferous kimberlites (Fig. 15c, f and k), and those actually included in diamonds. The most Cr-rich of these are the most Cr-rich spinels found in nature.

Spinels in lamproites and other highly potassic lavas also show wide scatter, and generally high values of Cr/(Cr + Al) similar to those in kimberlites, but at somewhat lower Mg (Figs 14b and 15d, g and l). Magnesioferrites and Mg-bearing magnetites are very rare.

The wide scatter within this category, and particularly that in the alkali basalts, may be the result of a Cr–Al trend being overprinted by a strong kimberlite trend. Furthermore, all of these lava types are commonly associated with deep-seated mantle or lower-crustal xenoliths, and part of the population of spinels, and particularly the Cr–Al trend, may be derived from disaggregated xenoliths.

Armstrong *et al.* (1995) explained the tendency for spinels in kimberlites to be oxidized by a mechanism of volatile evolution and oxidation upon intrusion into the crust. There may be a simpler explanation, however. The tendency for spinels in both alkali basalts and kimberlite to have higher ferric iron is more probably related to the strong influence that alkalis have on increasing the ferric/ferrous iron ratio of basic melts (Thornber *et al.*, 1980; Kilinc *et al.*, 1983; Carmichael, 1991).

Komatiites

The komatiite dataset is complicated by the generally high degree of alteration and metamorphism of most

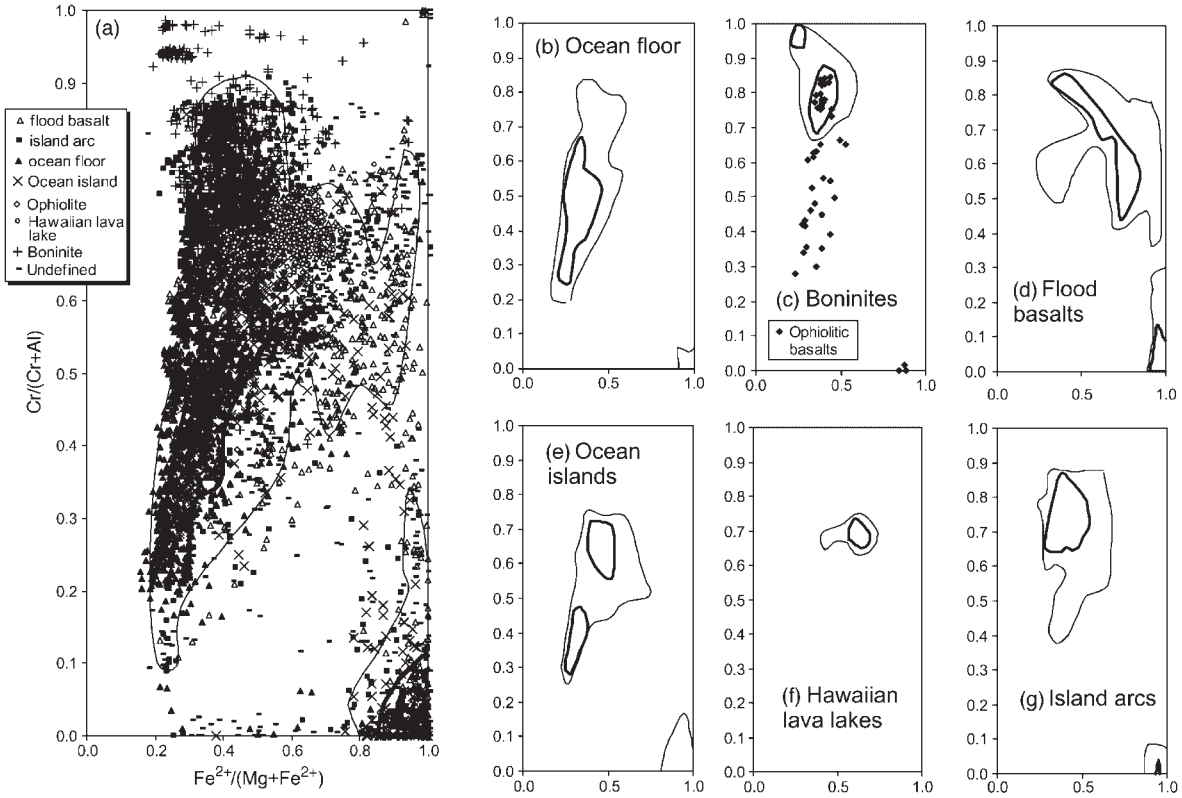

Fig. 12. Cr/(Cr + Al) vs $Fe^{2+}/(Mg + Fe^{2+})$ plot for tholeiitic basalts and boninites; subcategories as in Fig. 10.

komatiites, which is typically accompanied by extensive development of rims of metamorphic chromian magnetite or 'ferritchromit' (Barnes, 2000). This results in a large density of data points along the Cr–Fe^{3+} join, distinct from igneous magnetite compositions in being very low in Al. With the exception of Fig. 16e, which is included for purposes of comparison, metamorphic magnetite rims have been excluded (as far as possible) from the plots in Figs 16–18, which include only rim-free greenschist facies grains and cores of composite chromite–magnetite grains. Metamorphic magnetite compositions are considered under a separate heading below. In addition, the komatiite dataset also includes a large number of analyses of magnetites and ferrian chromites associated with the margins of massive sulphide deposits (Figs 16f and 17e and i)—these are greatly over-represented compared with their abundance in nature, and hence a DDCP for the komatiite dataset as a whole is not meaningful.

Cores of komatiitic chromites are tightly clustered close to the Cr apex on the triangular plot (Fig. 16), but show a very wide range in $Fe^{2+}/(Mg + Fe^{2+})$ at roughly constant Cr/(Cr + Al) and $Fe^{3+}/(Cr + Al + Fe^{3+})$ (Fig. 17) as a result of postcumulus, subsolidus and metamorphic Fe–Mg exchange. There is little difference in the distribution of points on the triangular plot between greenschist facies and amphibolite facies samples if only Al-undepleted komatiites (AUDK) are considered (Fig. 16b and c), although Barnes (2000) showed that there is some tendency towards Al depletion in chromite cores in lower to mid-amphibolite facies metamorphism where extensive fluid infiltration has taken place. Al-depleted komatiites (ADK) from amphibolite facies terrains (Fig. 16d) contain chromite with a significantly lower Al content, a feature that is probably inherited from the original magma composition. However, this population is overwhelmingly from one greenstone belt, the Forrestania Belt in Western Australia, which is metamorphosed to a higher grade (mid–upper amphibolite) than all of the other localities represented. No analyses are available from Al-depleted komatiites at sub-amphibolite metamorphic grades, so this conclusion remains to be fully tested.

Ti contents of komatiitic chromites are generally low (Fig. 18), but elevated concentrations do occur in chromites from slowly cooled orthocumulate rocks (Barnes,

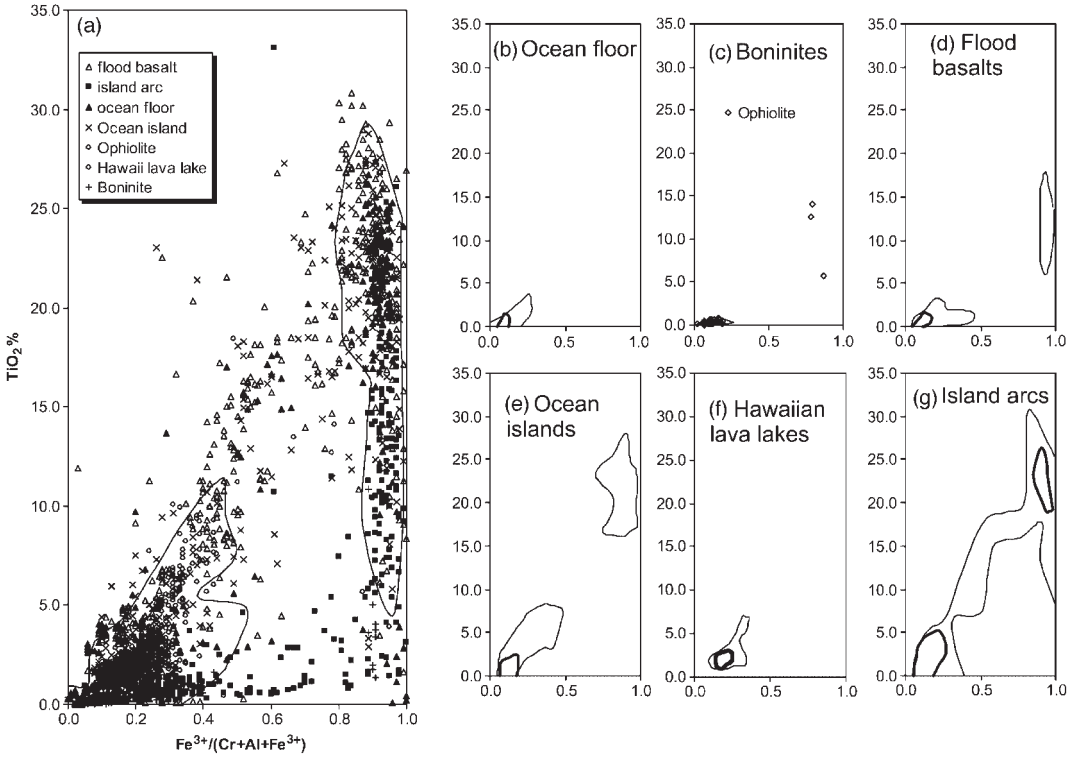

Fig. 13. TiO_2 vs $Fe^{3+}/(Cr + Al + Fe^{3+})$ plot for tholeiitic basalts and boninites; subcategories as in Fig. 10.

1998). The Fe–Ti trend is commonly developed in chromites from this environment.

Spinels associated with margins of massive sulphide orebodies in komatiites have distinctive and unique chemistry (Figs. 16f and 17e and i). They span most of the $Cr–Fe^{3+}–Fe^{2+}$ join of the spinel prism, clustering at the Cr-rich end of the trend, have very high $Cr/(Cr + Al)$, very high $Fe^{3+}/(Cr + Al + Fe^{3+})$ and contain a range of TiO_2 contents elevated relative to other komatiitic chromites but generally <2% (Fig. 18e). They overlap the field for Cr-rich metamorphic magnetite overgrowths in amphibolite facies rocks (compare Fig. 16e and f), but the more Cr-rich compositions (which account for >50% of the population) are unique among naturally occurring spinels. The group as a whole is completely distinct from all other igneous spinel groups.

Metamorphic spinels

Part of the bimodality in nature between chromites and magnetites is due to the presence of metamorphic magnetite rims on chromite grains in many metamorphosed ultramafic rocks (Onyeagocha, 1974; Bliss & MacLean, 1975; Abzalov, 1998; Barnes, 2000; among many other references). The $Cr/(Cr + Al)$ of primary igneous magnetite is distinct from that of magnetite modified by metamorphism. The $Cr/(Cr + Al)$ is low for primary igneous magnetite, because at the stage when magnetite appears on the liquidus of mafic magmas there is little Cr (Cr <100 ppm) but still a significant amount of Al present in the melt. Thus primary igneous magnetite plots at the lower right of $Cr/(Cr + Al)$ vs $Fe^{2+}/(Fe^{2+} + Mg)$ and along the $Al–Fe^{3+}$ join of $Cr–Al–Fe^{3+}$. Magnetite and chromite tend to lose Al, relative to Cr, during metamorphism and reaction with silicates and metamorphic fluids to form chlorite or amphibole, and the resulting spinel plots along the $Cr–Fe^{3+}$ join of $Cr–Al–Fe^{3+}$ and at the top right of $Cr/(Cr + Al)$ vs $Fe^{2+}/(Fe^{2+} + Mg)$. The low-alumina chromite resulting from metamorphism is often called 'ferritchromit'. Figure 19 shows DDCPs for spinels of metamorphic origin, including magnetite and ferritchromit rims (referred to from here on together as 'magnetite rims') (Fig. 19a, b, g, h, k and l), and metamorphogenic spinels from high-grade metasedimentary rocks or other metamorphic rocks of unknown protolith (Fig. 19d, f and j). Magnetite rims and metamorphic spinels define two completely distinct trends, the latter being dominated by Mg–Fe–Al spinels

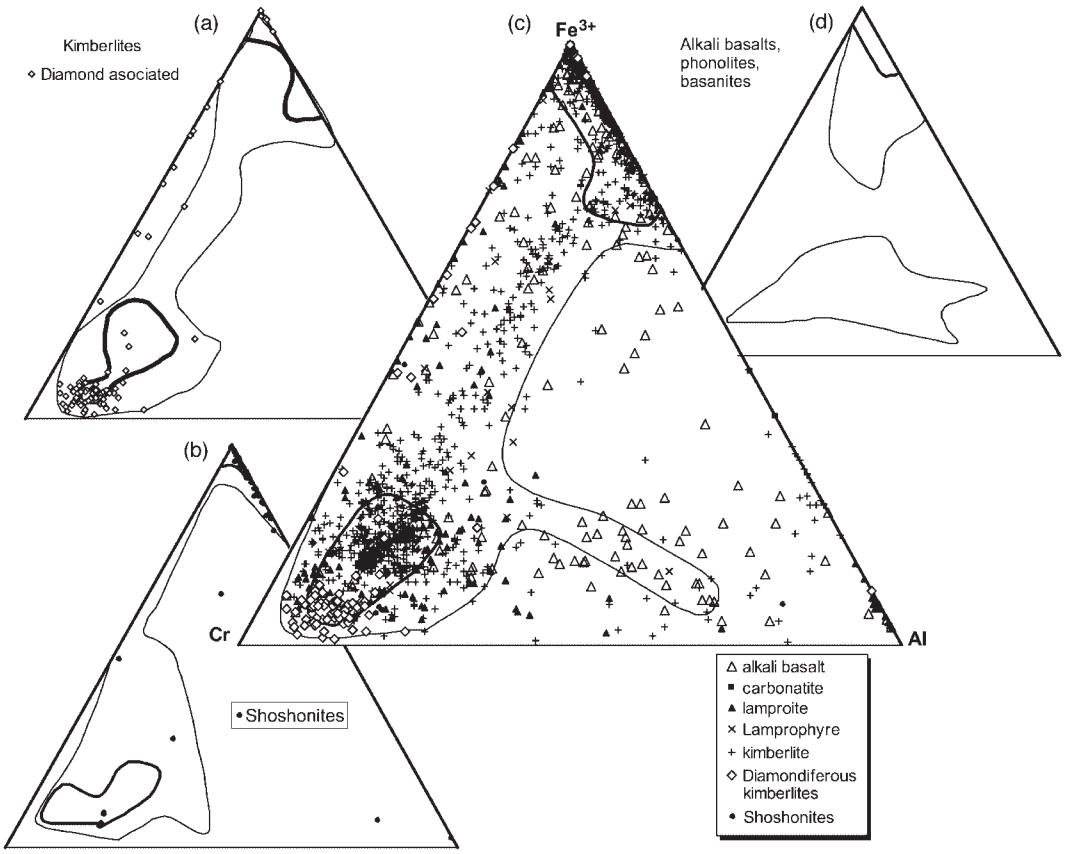

Fig. 14. Trivalent ion plots for alkali basalts, lamprophyres and related rocks, excluding samples identified as xenoliths or nodules. (a) Kimberlites, contours for entire dataset, diamond-associated kimberlites identified as individual data points; (b) lamproites (contoured), plus individual data points for shoshonites and other ultrapotassic magmas; (c) entire dataset; (d) alkali basalts, phonolites and basanites.

(and also including other more exotic species such as gahnites), generally close to the Al apex or along the Cr–Al join. These compositions are controlled by high-*P* metamorphic reactions involving Cr–Al–Fe-bearing silicates such as pyroxenes and garnets.

The 'magnetite rims' population discussed here is restricted to komatiitic rocks, although similar rims can be found in ultramafic rocks of any paragenesis. (Only the komatiitic examples could readily be identified within the database.) Rims are almost entirely restricted to the Cr–Fe^{3+} join (Fig. 19a and b), and those in greenschist facies rocks are dominated by nearly pure magnetites (Fig. 19b). At higher grades rims become characteristically zoned from Cr-poor margins to Cr-rich compositions at the inner contact with the chromite core. Barnes (2000) suggested that the maximum Cr content of the rims is controlled by equilibrium with chromite cores across the miscibility gap between chromite and magnetite, which widens rapidly below 600°C (Sack & Ghiorso, 1991).

The distribution of natural data suggests that the true picture may be more complex. There is a bimodality between Cr-bearing magnetites and 'ferritchromits' plotting midway along the Cr–Fe^{3+} join (Fig. 19a), which suggests that there may be an additional miscibility gap in natural spinels between these compositions. Further evidence for this in nature is the relatively rare but widespread occurrence of metamorphosed chromites where the chromite core is separated from the Cr-poor magnetite rim by an intervening sharply bounded zone of ferritchromit. Further work is clearly needed to elucidate the complex thermodynamics of the spinel solid solution at metamorphic temperatures.

DISCUSSION

The implications of global variability in spinel compositions have been discussed generally by Roeder (1994), and in relation to spinels in basalts by a number of

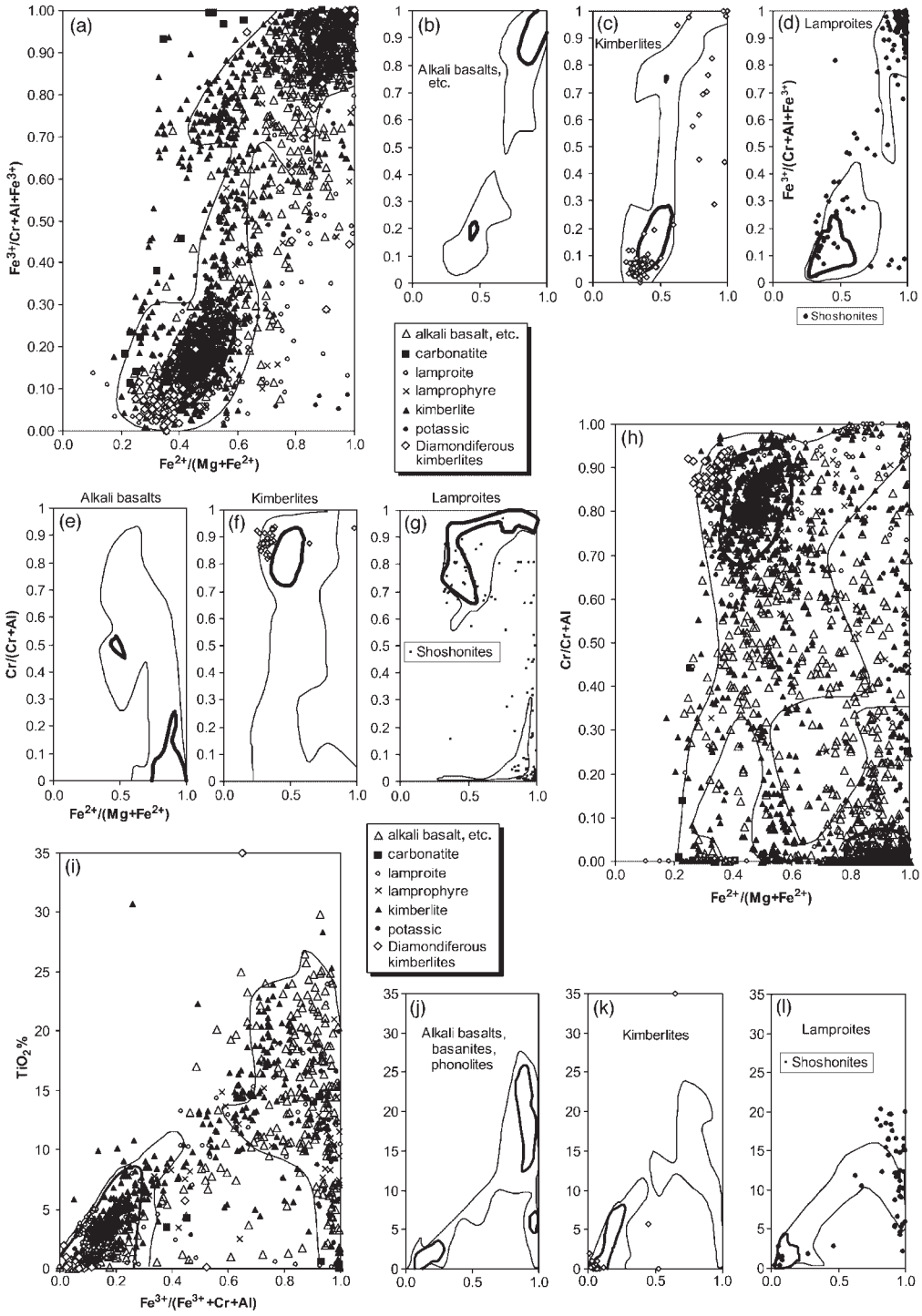

Fig. 15. $Fe^{3+}/(Cr + Al + Fe^{3+})$ vs $Fe^{2+}/(Mg + Fe^{2+})$, $Cr/(Cr + Al)$ vs $Fe^{2+}/(Mg + Fe^{2+})$ and TiO_2 vs $Fe^{3+}/(Cr + Al + Fe^{3+})$ for alkali basalts, lamprophyres and related rocks; subcategories as in Fig. 14.

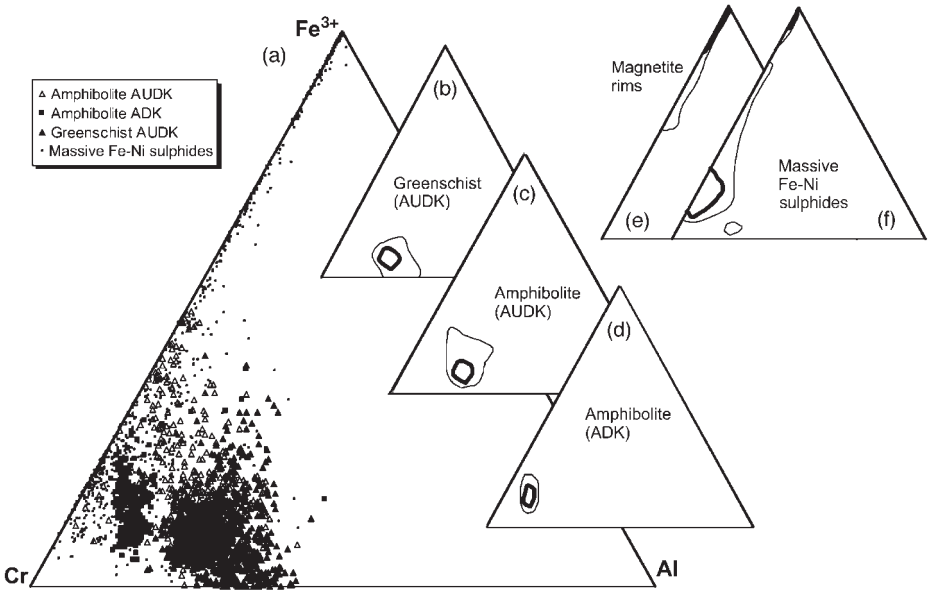

Fig. 16. Trivalent ion plots for komatiites (magnetite rims excluded). ADK, aluminium-depleted komatiites; AUDK, aluminium-undepleted komatiites. (a)–(d) exclude metamorphogenic magnetite rims. (b) Greenschist facies AUDK; (c) amphibolite facies AUDK; (d) amphibolite facies ADK; (e) metamorphogenic magnetite rims, all metamorphic grades; (f) spinels from margins of massive Ni–Fe sulphide orebodies.

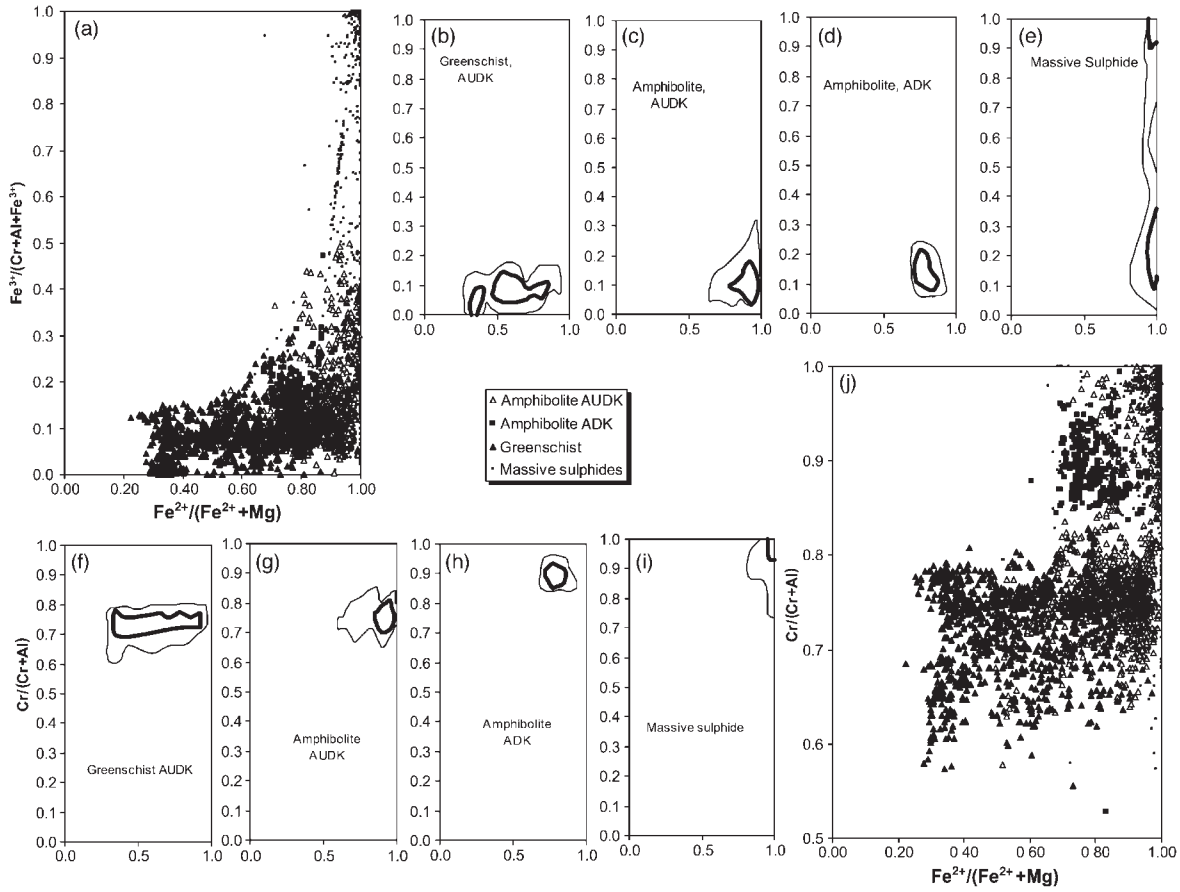

Fig. 17. $Fe^{3+}/(Cr + Al + Fe^{3+})$ vs $Fe^{2+}/(Mg + Fe^{2+})$ and $Cr/(Cr + Al)$ vs $Fe^{2+}/(Mg + Fe^{2+})$ for komatiites (magnetite and ferritchromit rims excluded); subcategories as in Fig. 16.

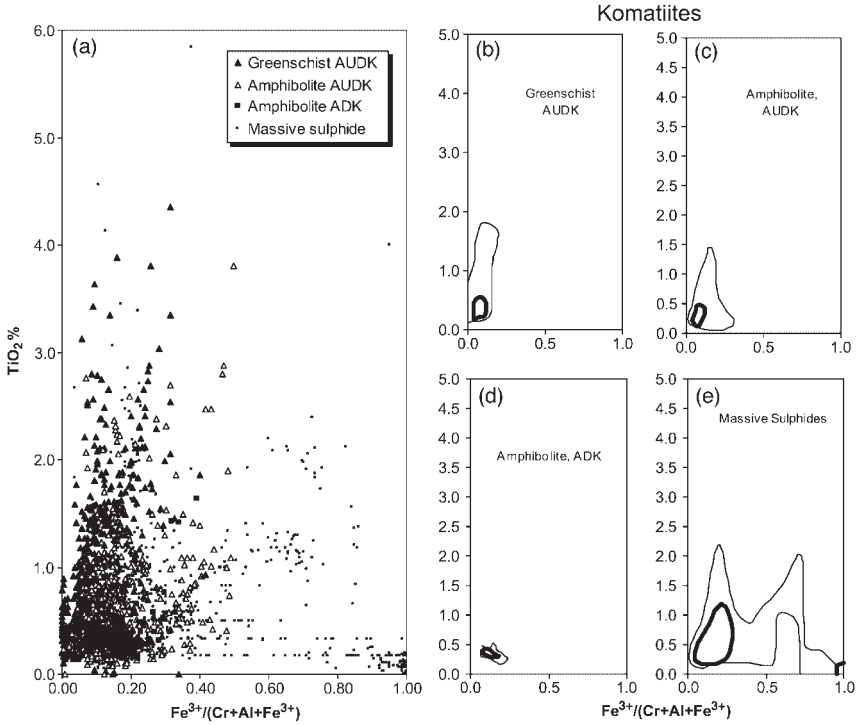

Fig. 18. TiO_2 vs $Fe^{3+}/(Cr + Al + Fe^{3+})$ plot for komatiites (magnetite rims excluded); subcategories as in Fig. 16.

workers (Dick & Bryan, 1978; Dick & Bullen, 1984; Roeder & Reynolds, 1991; Arai, 1992; Kamenetsky & Crawford, 1998; Kamenetsky *et al.*, 2001). The data compilation presented here allows meaningful global comparisons to made between different magma types and sources, with broad petrogenetic implications.

Ophiolitic basalts, boninites and chromitites

There is a strong affinity between ophiolites and boninites, and a significant proportion of basalts associated with ophiolite complexes have been identified as boninites (Cameron, 1985, 1989; Coish, 1989). Spinels from unclassified ophiolitic basalts overlap strongly with those from known boninites (Figs 10–13), implying that many of these basalts are boninites as well. This raises the question of whether boninites are the dominant parent magma for podiform chromite deposits in ophiolites. These chromitites have somewhat intermediate characteristics between the boninite and MORB fields (Fig. 20), with a generally closer similarity to boninites but slightly lower Fe^{3+} and a wider range in $Cr/(Cr + Al)$ extending to less Cr-rich compositions. All groups are very low in Ti. Boninites are the only group of natural magmas, excluding kimberlites and komatiites, that *commonly* contain spinels as Cr rich as those typical of ophiolitic chromitites (Fig. 20). This implies that the 'average' parental magma to ophiolitic chromitites is towards the boninite end of a MORB–boninite spectrum.

The question remains of why boninites contain such Cr-rich spinels compared with all other known mafic lavas. The answer may lie partly in their derivation from very highly depleted and consequently Al-poor mantle (Crawford & Cameron, 1985; Sobolev & Danyushevsky, 1994), but MORBs are also derived from depleted mantle and only rarely contain chromites Cr-rich enough to overlap the boninite field. Komatiites also represent high-degree partial melts of depleted mantle, have high ratios of Cr to Al in the melt, and might be expected to have significantly more Cr-rich chromites than boninites, whereas in fact the spinel populations are fairly similar.

Boninites have the distinguishing characteristic of high primary water content, resulting in the suppression of the silicate liquidus. This may result in early crystallization of spinel relative to Cr-bearing pyroxenes, compared with the sequence in water-poor mafic melts (Bannister *et al.*, 1998).

Whatever the explanation, a connection with the subduction environment is strongly suggested. The only other mafic lavas in nature that *commonly* contain chromites with $Cr/(Cr + Al) > 0{\cdot}75$ and $Fe^{2+}/(Mg + Fe^{2+}) < 0{\cdot}6$ are from island arcs or back-arc basins, notably the Lau Basin (Allan, 1994). Hydrous melting of highly depleted

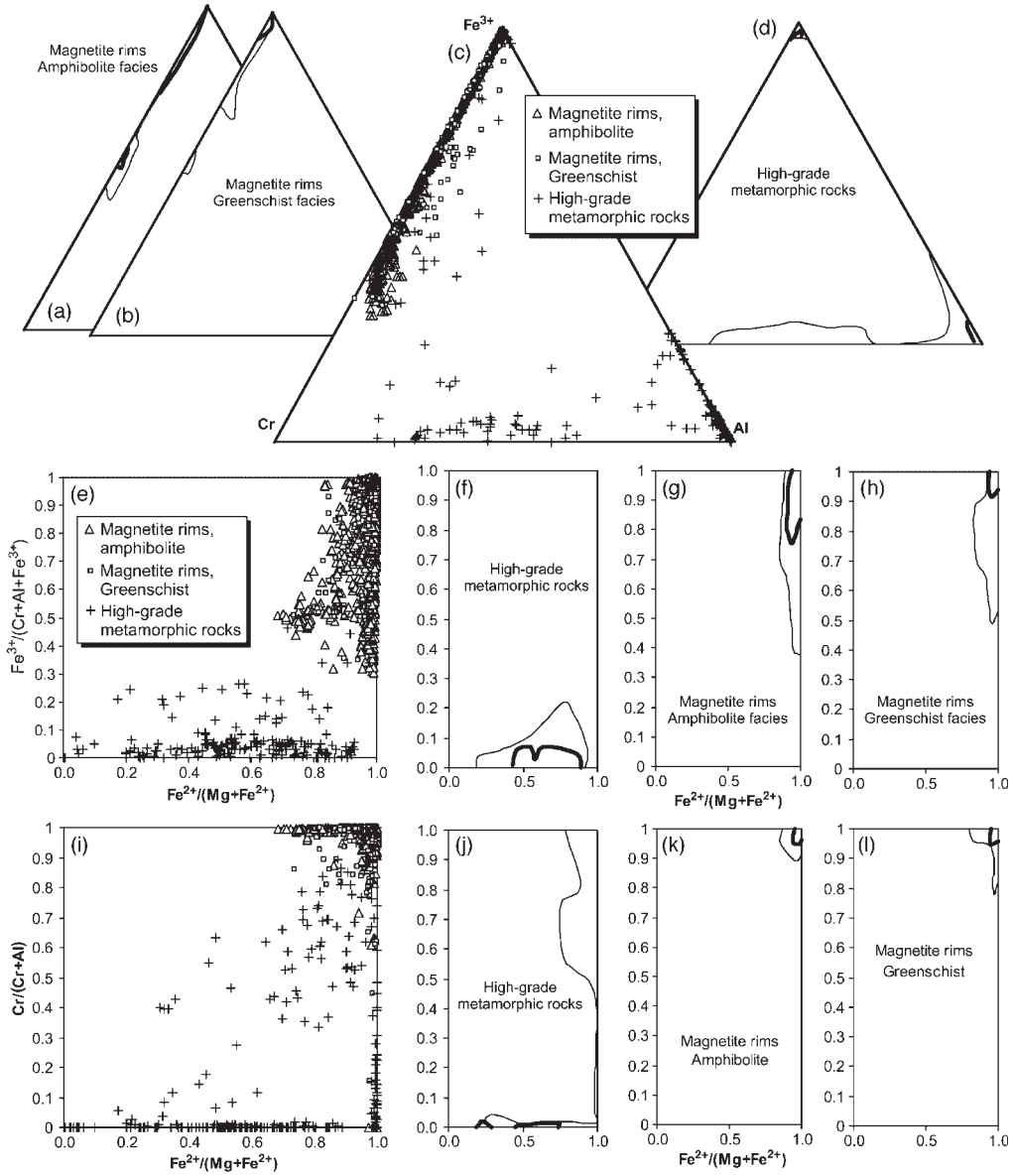

Fig. 19. Trivalent ion, $Fe^{3+}/(Cr + Al + Fe^{3+})$ vs $Fe^{2+}/(Mg + Fe^{2+})$ and $Cr/(Cr + Al)$ vs $Fe^{2+}/(Mg + Fe^{2+})$ plots for metamorphic spinels, and magnetite and ferritchromit rims. (a), (b), (g), (h), (k) and (l), magnetite rims from komatiites; (c), (e) and (i), all data points; (d), (f) and (j), spinels from high-grade metasedimentary rocks

sources is favoured as the explanation for the distinctive characteristics of boninitic chromites.

Cr-rich, Fe^{3+}-poor chromites in komatiites

Cr- and Mg-rich chromites, reflecting primary crystallization from primitive, unfractionated mantle-derived magmas, are known from komatiites as well as from boninites and ophiolites (Fig. 20b). The most Cr-rich grouping of spinels found in nature (excluding chromite inclusions in diamonds) are those from Al-depleted komatiites (Fig. 20b), with boninites a very close second. In both cases the high Cr can be attributed to melt composition, both magma types having high Cr:Al ratios. In the case of boninites this is due to previous depletion of the mantle source, whereas in Al-depleted komatiites it is due to Al retention by majorite garnet in the source (Ohtani *et al.*, 1988; Fan & Kerrich, 1997; Inoue *et al.*, 2000).

Komatiitic chromites, particularly those from large olivine-rich lava channels formed from Al-undepleted

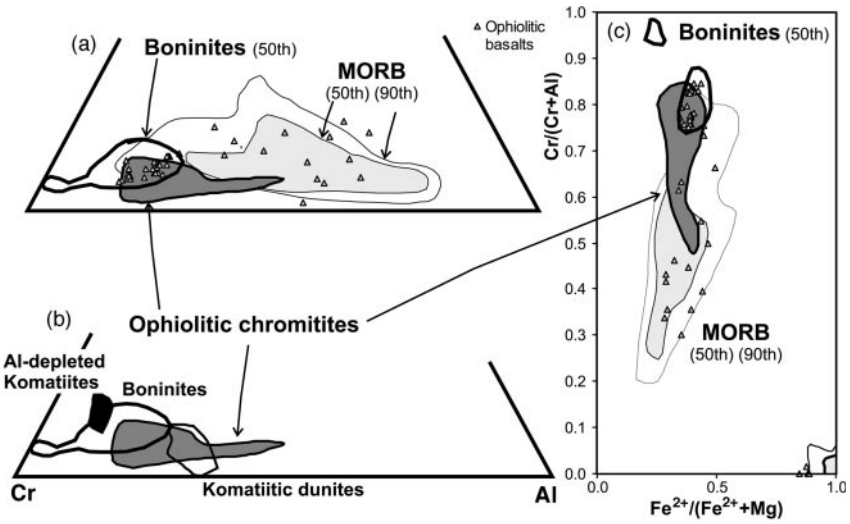

Fig. 20. Compositions of chromites from boninites (ophiolite and ocean-floor samples), mid-ocean ridge basalts and ophiolitic chromitites (50th percentiles). Individual data points are boninites from ophiolite complexes and uncharacterized basalts (which may or may not be boninites) from ophiolites.

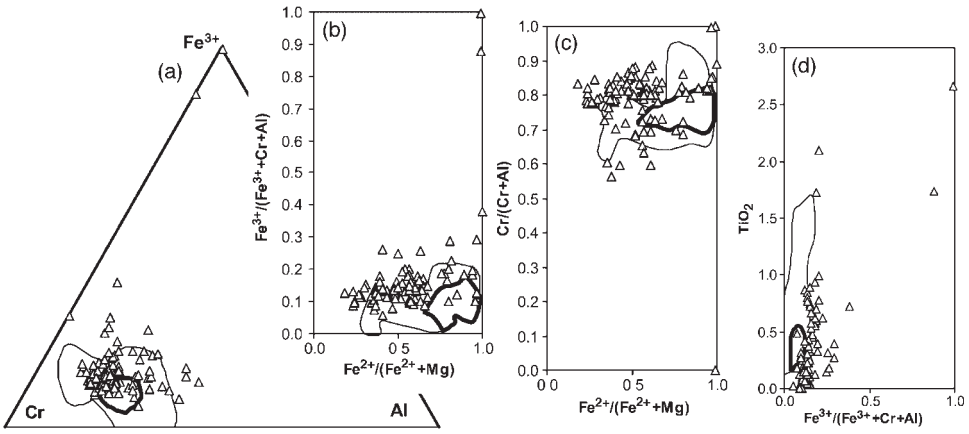

Fig. 21. Comparison of data points from Witwatersrand conglomerates with 50th and 90th percentiles for all chromite cores from komatiites.

komatiites (Barnes, 1998), are among the most reduced found in terrestrial igneous rocks (Fig. 20b). Relatively unaltered chromites with very low Fe^{3+} contents are found in essentially unmetamorphosed komatiitic dunites, indicating that these are primary liquidus compositions recording very primitive magmas. The highly reduced nature of these komatiitic chromites is attributed to magma composition, and may ultimately reflect the nature of the mantle source. The only comparably reduced chromites in nature are those from ophiolitic chromitites, which by virtue of their nearly monomineralic nature also preserve primitive liquidus compositions. Komatiites and the parent magmas to ophiolitic cumulates formed from high degrees of melting of reduced, depleted mantle.

Source of Witwatersrand spinels

Compositions of detrital spinels from the auriferous Witwatersrand conglomerates (Viljoen & van der Walt, 1973) are compared with komatiite chromite fields in Fig. 21. These chromites show a closer correspondence to komatiitic chromites than any other data grouping, and this comparison supports the derivation of these grains from komatiites in an Archaean volcanic terrain.

Cr/(Cr + Al) ratios are slightly high compared with average komatiites, implying that the source rocks were Al-depleted komatiites, consistent with the occurrence of this type of komatiite in the early Archaean hinterland.

CONCLUSION

Spinel compositions in terrestrial rocks show a remarkably wide range of variation, attributable to a spectrum of igneous processes with superimposed metamorphic effects. Perhaps the most striking variability is found in spinels in different types of mafic lavas: continental flood basalts, ocean-floor basalts and boninites (to take the most contrasting groups) have entirely different spinel populations despite broadly overlapping ranges in major element chemistry. Processes of high- and low-pressure crystal fractionation and crustal contamination are recorded by the spinel chemistry.

Chromium-rich, Mg-rich chromites are the hallmark of primitive mantle-derived magmas that have not undergone these overprints. They are found within boninites, ophiolitic cumulates, kimberlites and komatiites, but relatively rarely within basalts. The global distribution of spinel compositions is influenced greatly by the rarity of preservation of primitive mantle melts.

The global spinel database has great potential to be used in investigations of petrogenesis and provenance. Many factors must be taken into account, particularly the tendency of chromites to re-equilibrate with surrounding silicates during prolonged cooling and metamorphism. With this reservation in mind, many possible applications exist.

ACKNOWLEDGEMENTS

We thank Dr Alexei Poustovetov for his constructive comments on a preliminary draft of this paper, and Professor R. Arculus and Dr D. Kamenetsky for very helpful reviews.

REFERENCES

Abzalov, M. Z. (1998). Chrome-spinels in gabbro–wehrlite intrusions of the Pechenga area, Kola Peninsula, Russia: emphasis on alteration features. *Lithos* **43**, 109–134.

Allan, J. F. (1994). Cr-spinel in depleted basalts from the Lau Basin backarc: petrogenetic history from Mg–Fe crystal–liquid exchange. In: Hawkins, J. W., Parson, L. M. *et al.* (eds) *Proceedings of the Ocean Drilling Program, Scientific Results, 135*. College Station, TX: Ocean Drilling Program, pp. 565–583.

Arai, S. (1992). Chemistry of chromian spinel in volcanic rocks as a potential guide to magma chemistry. *Mineralogical Magazine* **56**, 173–184.

Armstrong, K. A., Roeder, P. L. & Helmstaedt, H. H. (1995). An investigation of the spinel mineralogy of the C14 kimberlite, Kirkland Lake, Ontario. *Proceedings of the International Kimberlite Conference* **6**, 14–16.

Bannister, V., Roeder, P. & Poustovetov, A. (1998). Chromite in the Paricutin lava flows (1943–1952). *Journal of Volcanology and Geothermal Research* **87**, 151–171.

Barnes, S. J. (1998). Chromite in komatiites, 1. Magmatic controls on crystallization and composition. *Journal of Petrology* **39**, 1689–1720.

Barnes, S. J. (2000). Chromite in komatiites, II. Modification during greenschist to mid-amphibolite facies metamorphism. *Journal of Petrology* **41**, 387–409.

Barnes, S. J. & Kunilov, V. Y. (2000). Chrome spinels and Mg-ilmenites from the Noril'sk 1 and Talnakh intrusions and other mafic rocks of the Siberian flood basalt province. *Economic Geology* **95**, 1701–1717.

Bliss, N. W. & MacLean, W. H. (1975). The paragenesis of zoned chromite from central Manitoba. *Geochimica et Cosmochimica Acta* **39**, 973–990.

Bonatti, E. & Michael, P. J. (1989). Mantle peridotites from continental rifts to ocean basins to subduction zones. *Earth and Planetary Science Letters* **91**, 297–311.

Cameron, W. E. (1985). Petrology and origin of primitive lavas from the Troodos ophiolite, Cyprus. *Contributions to Mineralogy and Petrology* **89**, 239–255.

Cameron, W. E. (1989). Contrasting boninite–tholeiite association from New Caledonia. In: *Boninites and Related Rocks*. London: Unwin Hyman, pp. 314–338.

Carmichael, I. S. E. (1991). The redox states of basic and silicic magmas: a reflection of their source regions? *Contributions to Mineralogy and Petrology* **106**, 129–141.

Cawthorn, R. G., De Wet, M., Hatton, C. J. & Cassidy, K. F. (1991). Ti-rich chromite from the Mount Ayliff intrusion, Transkei: further evidence for high Ti tholeiitic magma. *American Mineralogist* **76**, 561–573.

Coish, R. A. (1989). Boninitic lavas in Appalachian ophiolites: a review. In: *Boninites and Related Rocks*. London: Unwin Hyman, pp. 264–287.

Crawford, A. J. & Cameron, W. E. (1985). Petrology and geochemistry of Cambrian boninites and low-Ti andesites from Heathcote, Victoria. *Contributions to Mineralogy and Petrology* **91**, 93–104.

Dick, H. J. B. & Bryan, W. B. (1978). Variation of basalt phenocryst mineralogy and rock compositions in DSDP Hole 396B. In: Dmitriev, L., Heirtzler, J. *et al.* (eds) *Initial Reports of the Deep Sea Drilling Project, 46*. Washington, DC: US Government Printing Office, pp. 215–225.

Dick, H. J. B. & Bullen, T. (1984). Chromian spinel as a petrogenetic indicator in abyssal and alpine-type peridotites and spatially associated lavas. *Contributions to Mineralogy and Petrology* **86**, 54–76.

Eales, H. V. (1979). Anomalous Karoo spinels along the chromite–titanomagnetite join. *South African Journal of Science* **75**, 24–29.

Fan, J. & Kerrich, R. (1997). Geochemical characteristics of aluminum depleted and undepleted komatiites and HREE-enriched low-Ti tholeiites, western Abitibi greenstone belt—a heterogeneous mantle plume convergent margin environment. *Geochimica et Cosmochimica Acta* **61**, 4723–4744.

Henderson, P. (1975). Reaction trends shown by chrome-spinels of the Rhum layered intrusion. *Geochimica et Cosmochimica Acta* **39**, 1035–1044.

Henderson, P. & Wood, R. J. (1981). Reaction relationships of chrome-spinels in igneous rocks—further evidence from the layered intrusions of Rhum and Mull, Inner Hebrides, Scotland. *Contributions to Mineralogy and Petrology* **78**, 225–229.

Inoue, T., Rapp, R. P., Zhang, J. Z., Gasparik, T., Weidner, D. J. & Irifune, T. (2000). Garnet fractionation in a hydrous magma ocean and the origin of Al-depleted komatiites: melting experiments of

hydrous pyrolite with REEs at high pressure. *Earth and Planetary Science Letters* **177**, 81–87.

Irvine, T. N. (1965). Chromian spinel as a petrogenetic indicator. Part I. Theory. *Canadian Journal of Earth Sciences* **2**, 648–672.

Irvine, T. N. (1967). Chromian spinal as a petrogenetic indicator, part 2. Petrologic applications. *Canadian Journal of Earth Sciences* **4**, 71–103.

Irvine, T. N. (1977). Origin of chromitite layers in the Muskox Intrusion and other stratiform intrusions: a new interpretation. *Geology* **5**, 273–277.

Kamenetsky, V. S. & Crawford, A. J. (1998). Melt–peridotite reaction recorded in the chemistry of spinel and melt inclusions in basalt from 43 degrees N, Mid-Atlantic Ridge. *Earth and Planetary Science Letters* **164**, 345–352.

Kamenetsky, V. S., Crawford, A. J. & Meffre, S. (2001). Factors controlling chemistry of magmatic spinel: an empirical study of associated olivine, Cr-spinel and melt inclusions from primitive rocks. *Journal of Petrology* **42**, 655–671.

Kilinc, A., Carmichael, I. S. E., Rivers, M. L. & Sack, R. O. (1983). The ferric–ferrous ratio of natural silicate liquids equilibrated in air. *Contributions to Mineralogy and Petrology* **83**, 136–140.

Mattioli, G. S. & Wood, B. J. (1988). Magnetite activities across the $MgAl_2O_4$–Fe_3O_4 spinel join, with application to thermobarometric estimates of the upper mantle oxygen fugacity. *Contributions to Mineralogy and Petrology* **98**, 148–162.

Nell, J. & Wood, B. J. (1989). Thermodynamic properties in a multicomponent solid solution involving cation disorder: Fe_3O_4–$MgFe_2O_4$–$FeAl_2O_4$–$MgAl_2O_4$ spinels. *American Mineralogist* **74**, 1000–1015.

Ohtani, E., Moriyama, J. & Kawabe, I. (1988). Majorite garnet stability and its implications for the genesis of komatiite magmas. *Chemical Geology* **70**, 147–157.

O'Neill, H. S. C. & Wall, V. J. (1987). The olivine–orthopyroxene–spinel oxygen geobarometer, the nickel precipitation curve, and the oxygen fugacity of the Earth's upper mantle. *Journal of Petrology* **28**, 1169–1191.

Onyeagocha, A. C. (1974). Alteration of chromite from the Twin Sisters dunite, Washington. *American Mineralogist* **59**, 608–612.

Poustovetov, A. A. (2000). Numerical modeling of chemical equilibria between chromian spinel, olivine, and basaltic melt, with petrologic applications. Ph.D. thesis, Queen's University, Kingston, Ontario, 135 pp.

Power, M. R., Pirrie, D., Andersen, J. C. O. & Wheeler, P. D. (2000). Testing the validity of chrome spinel chemistry as a provenance and petrogenetic indicator. *Geology* **28**, 1027–1030.

Rock, N. M. S. (1986). The nature and origin of ultramafic lamprophyres: alnoites and allied rocks. *Journal of Petrology* **27**, 155–196.

Roeder, P. L. (1994). Chromite: from the fiery rain of chondrules to the Kilauea Iki lava lake. *Canadian Mineralogist* **32**, 729–746.

Roeder, P. L. & Campbell, I. H. (1985). The effect of postcumulus reactions on compositions of chrome-spinels from the Jimberlana Intrusion. *Journal of Petrology* **26**, 763–786.

Roeder, P. L. & Reynolds, I. (1991). Crystallization of chromite and chromium solubility in basaltic melts. *Journal of Petrology* **32**, 909–934.

Roeder, P. L., Poustovetov, A. A. & Oskarsson, N. (2000). Growth forms and composition of chromian spinel in MORB magma: diffusion-controlled crystallization of chromian spinel. *Canadian Mineralogist* **39**, 397–416.

Sack, R. O. & Ghiorso, M. S. (1991). Chromian spinels as petrogenetic indicators: thermodynamic and petrological applications. *American Mineralogist* **76**, 827–847.

Scowen, P. A. H., Roeder, P. L. & Heltz, R. T. (1991). Reequilibration of chromite within Kilauea Iki lava lake, Hawaii. *Contributions to Mineralogy and Petrology* **107**, 8–20.

Sinton, J. M. (1977). Equilibration history of the basal alpine-type peridotite, Red Mountain, New Zealand. *Journal of Petrology* **18**, 216–246.

Sobolev, A. & Danyushevsky, L. V. (1994). Petrology and geochemistry of boninites from the north termination of the Tonga Trench: constraints on the generation conditions of primary high-Ca boninite magmas. *Journal of Petrology* **35**, 1183–1211.

Stevens, R. E. (1944). Compositions of some chromites of the western hemisphere. *American Mineralogist* **29**, 1–34.

Thornber, C. R., Roeder, P. L. & Foster, J. R. (1980). The effect of composition on the ferric–ferrous ratio in basaltic liquids at atmospheric pressure. *Geochimica et Cosmochimica Acta* **44**, 525–532.

Viljoen, E. A. & van der Walt, E. (1973). The composition of chromite grains from various Witwatersrand reefs. *National Institute for Metallurgy, South Africa, Report 1924*, 3–95.

Wood, B. J. (1990). An experimental test of the spinel peridotite oxygen barometer. *Journal of Geophysical Research* **95b**, 15845–15851.

Wood, B. J. & Virgo, D. (1989). Upper mantle oxidation state: ferric iron contents of lherzolite spinels by 57Fe Mossbauer spectroscopy and resultant oxygen fugacities. *Geochimica et Cosmochimica Acta* **53**, 1277–1291.